1995-06

Simulation of acoustic multipath arrival structure in the Middle Atlantic Bight

Kaemmerer, Glen E.

Monterey, California. Naval Postgraduate School

NAVAL POSTGRADUATE SCHOOL
MONTEREY, CALIFORNIA

THESIS

SIMULATION OF ACOUSTIC MULTIPATH ARRIVAL STRUCTURE IN THE MIDDLE ATLANTIC BIGHT

by

Glen E. Kaemmerer, Jr.

June, 1995

Thesis Advisors: James H. Miller
Ching-Sang Chiu
Kevin B. Smith

Approved for public release; distribution is unlimited.

REPORT DOCUMENTATION PAGE

Form Approved OMB No. 0704-0188

1. AGENCY USE ONLY *(Leave blank)*	2. REPORT DATE June 1995.	3. REPORT TYPE AND DATES COVERED Master's Thesis

4. TITLE AND SUBTITLE SIMULATION OF ACOUSTIC MULTIPATH ARRIVAL STRUCTURE IN THE MIDDLE ATLANTIC BIGHT	5. FUNDING NUMBERS
6. AUTHOR(S) Glen E. Kaemmerer, Jr.	
7. PERFORMING ORGANIZATION NAME(S) AND ADDRESS(ES) Naval Postgraduate School Monterey CA 93943-5000	8. PERFORMING ORGANIZATION REPORT NUMBER
9. SPONSORING/MONITORING AGENCY NAME(S) AND ADDRESS(ES)	10. SPONSORING/MONITORING AGENCY REPORT NUMBER

11. SUPPLEMENTARY NOTES The views expressed in this thesis are those of the author and do not reflect the official policy or position of the Department of Defense or the U.S. Government.

12a. DISTRIBUTION/AVAILABILITY STATEMENT Approved for public release; distribution is unlimited.	12b. DISTRIBUTION CODE

13. ABSTRACT *(maximum 200 words)*

In support of the Mid-Atlantic Bight Field Study process studies to be conducted in July 1996 and February 1997, a feasibility study and simulation of the acoustic multipath arrival structure was conducted. The feasibility study consisted of a literature search of oceanographic, geophysical and climatological data to create an accurate model of the Middle Atlantic Bight. This model was used to predict transmission losses and signal-to-noise ratios expected during the field study. Simulations were conducted by tracing acoustic rays from a 400 Hz tomographic source to a vertical receiver array over a range of 45 kilometers across the continental shelf. Simulations were performed using the NOAA Hamiltonian Raytracing Program for the Ocean (HARPO) with the modeled ocean as input. Optimal placement of the experiment's components were determined. Ray path and arrival structure were examined through the construction of eigenrays and analysis of arrival depths, times, angles amplitudes. An analysis of the resolvability of individual rays utilizing arrival times and a combination of arrival times and angles was conducted to evaluate the feasibility of the tomography experiment in the Middle Atlantic Bight.

14. SUBJECT TERMS Acoustic Tomography, Ocean Acoustics, Oceanography, Middle Atlantic Bight			15. NUMBER OF PAGES 83
			16. PRICE CODE
17. SECURITY CLASSIFICATION OF REPORT Unclassified	18. SECURITY CLASSIFICATION OF THIS PAGE Unclassified	19. SECURITY CLASSIFICATION OF ABSTRACT Unclassified	20. LIMITATION OF ABSTRACT UL

NSN 7540-01-280-5500 Standard Form 298 (Rev. 2-89)

Prescribed by ANSI Std. 239-18 298-102

Approved for public release; distribution is unlimited.

SIMULATION OF ACOUSTIC
MULTIPATH ARRIVAL STRUCTURE
IN THE MIDDLE ATLANTIC BIGHT

Glen E. Kaemmerer, Jr.
Lieutenant Commander, United States Navy
B.S., University of Illinois, 1982

Submitted in partial fulfillment
of the requirements for the degree of

MASTER OF SCIENCE IN APPLIED PHYSICS

from the

NAVAL POSTGRADUATE SCHOOL
June 1995

Author: [redacted]
Glen E. Kaemmerer, Jr.

Approved by: [redacted]
James H. Miller, Thesis Advisor

[redacted]
Ching-Sang Chiu, Thesis Co-Advisor

[redacted]
Kevin B. Smith, Thesis Co-Advisor

[redacted]
William B. Colson, Chairman
Department of Physics

ABSTRACT

In support of the Mid-Atlantic Bight Field Study process studies to be conducted in July 1996 and February 1997, a feasibility study and simulation of the acoustic multipath arrival structure was conducted. The feasibility study consisted of a literature search of oceanographic, geophysical and climatological data to create an accurate model of the Middle Atlantic Bight. This model was used to predict transmission losses and signal-to-noise ratios expected during the field study. Simulations were conducted by tracing acoustic rays from a 400 Hz tomographic source to a vertical receiver array over a range of 45 kilometers across the continental shelf. Simulations were performed using the NOAA Hamiltonian Raytracing Program for the Ocean (HARPO) with the modeled ocean as input. Optimal placement of the experiment's components were determined. Ray path and arrival structure were examined through the construction of eigenrays and analysis of arrival depths, times, angles amplitudes. An analysis of the resolvability of individual rays utilizing arrival times and a combination of arrival times and angles was conducted to evaluate the feasibility of the tomography experiment in the Middle Atlantic Bight.

TABLE OF CONTENTS

LIST OF FIGURES

LIST OF TABLES

ACKNOWLEDGEMENTS

I would like to take this opportunity to express my sincere gratitude and appreciation to several people who helped me throughout this thesis project. I would like to thank my thesis advisors, Professors Jim Miller, Ching-Sang Chiu and Kevin Smith for their guidance, insight and inspiration. Jim's patience, understanding and easy-going attitude made the task-in-hand a more pleasurable experience. Ching-Sang provided the necessary tools (HARPO) to complete the project and gave me those often needed reality checks. Kevin, who joined the Naval Postgraduate School staff and tomography team midway through my research, provided a physicist's point of view and valuable details which were incorporated into the final product.

I would like to thank my fellow thesis group student Jeff Benson for providing helpful insight in the preparation of my HARPO input files and keeping me motivated throughout the project. To the remainder of group, Bob Staten, Don Taube and Tony D'Agostino, thanks for the encouragement and keeping my spirits up. To the computer experts of the COAC lab, Stefan Hudson and Carl Forsythe, thanks for all of your computer help. I especially need to thank Chris Miller who often put his own work aside to provide insight and answer my numerous questions on tomography, signal processing and computers, to name a few. Not only did he provide a wealth of technical information, he became a good friend. His assistance was most significant to the completion of this project.

I would also like to thank Kurt and Kathy Beernink who assisted in the collection of the background oceanographic data and with the word processing required to put this product in its final format. Their friendship over the years is truly treasured.

Finally, and most importantly, I wish to thank my wife Cindy and daughter Kimberly for their continued love, patience and support. Without them I could have never completed this project or my studies at the Naval Postgraduate School.

I. INTRODUCTION

A. OCEAN ACOUSTIC TOMOGRAPHY

Ocean acoustic tomography is a technique for observing the dynamic behavior of ocean processes by measuring the changes in travel time of acoustic signals transmitted over a number of ocean paths (Spindel, 1986). The concept was first proposed by Munk and Wunsch (1979) as a means of large scale monitoring of mesoscale processes and fluctuations in the ocean. Ocean acoustic tomography is analogous to the medical technique of using X-rays in Computer Assisted Tomography (CAT) scans or the geological process of using natural or manmade shock waves to explore the earth's interior. The word tomography is derived from two Greek roots meaning "to slice" and "to look at". Ocean acoustic tomography uses low frequency sound waves to "look at" a "slice" of the ocean by measuring the travel times of various signals travelling over different paths through the water. Speed of sound in the ocean is a function of temperature, salinity and depth. As sound waves travel in the ocean, they gather information about these parameters as well as current speeds and directions. The data is in the form of differences in the sound pulse travel times. These travel times contain a great deal of information and using mathematical inverse techniques an excellent estimate of the ocean structure can be constructed.

An ocean acoustic tomography experiment can be segmented into two separate and distinct parts. The first is the forward problem which establishes a physical relationship between the data and the unknown structure. The second is the inverse problem which deals with the reconstruction of the unknown environment based on the physical relationships developed in the forward problem. (Munk and Wunsch, 1979)

The feasibility of using acoustic tomography to monitor ocean conditions is determined by four important issues (Munk and Wunsch, 1979):

1. Stability
2. Resolvability
3. Identifiability
4. Signal-to-Noise Ratio

An eigenray is a path which directly connects a specific source with a specific receiver. This path must be stable to allow for long periods of unambiguous tracking of the ray arrivals. Resolvability requires that arrival time separation between eigenrays be large enough to resolve individual rays. The third requirement, identifiability, ensures that measured arrival times of eigenrays correspond to the modeled arrival times to determine the geometry of the acoustic paths. Finally, adequate signal-to-noise ratios ensure that signals are strong enough to be received over background noise.

Ocean acoustic tomography has several advantages over more traditional oceanographic methods (Chiu *et al.*, 1987):

1. A system can be implemented in the ocean on a semi-permanent basis for continuous observations.
2. It is not affected greatly by weather conditions.
3. It has high temporal resolution.
4. It can cover an extensive volume of the ocean interior and probe the different parts simultaneously.
5. Only a few moorings are needed, thus minimizing the effort in deployment and maintenance.

Originally, ocean acoustic tomography was primarily concentrated on deep ocean monitoring. In shallow water, the propagation of sound becomes more

complex and difficult to predict. Frequent interactions with the surface and bottom make multipath ray arrival difficult to track and times difficult to estimate. However in recent years with new naval battlefields extending into the littoral regions (O'Keefe *et al.*, 1992), tomography techniques have been adapted for studies in shallow coastal waters. The 1992 Barents Sea Polar Front Experiment, led by scientists and engineers from the Naval Postgraduate School and Woods Hole Oceanographic Institution, obtained successful results using shallow water techniques (Chiu, 1995) (Miller, 1995). The concentration of this thesis will be to utilize shallow water tomography techniques in support of the Mid-Atlantic Bight Field Study.

B. MID-ATLANTIC BIGHT FIELD STUDY

The Mid-Atlantic Bight Field Study is planned to be conducted over a two year period running from December 1995 to December 1997. The experiment will be conducted jointly by the Naval Postgraduate School and Woods Hole Oceanographic Institution. An integrated acoustic and oceanographic study, it will examine sound propagation from the continental slope to the continental shelf. The overall scientific goal of the proposed study is to quantify shelfbreak frontal variability and its coupling to the adjacent slope water circulation and to determine the impact of this variability on sound propagation from the continental slope onto the shelf. A practical motivation by the United States Navy of this study is to gain fundamental insights into acoustic propagation in the slope-shelf transition region and apply these insights to target detection and localization. (Chiu, 1994) As conditions at the shelfbreak differ drastically between seasons, two 3-week intensive process studies, one in July 1996 and one in February 1997, will be critical components of the entire study. These two process studies will be the concentration of this thesis.

Figure 1 shows the proposed location of the Mid-Atlantic Bight Field Study. The process studies will take place within an approximately 60 km x 20 km region

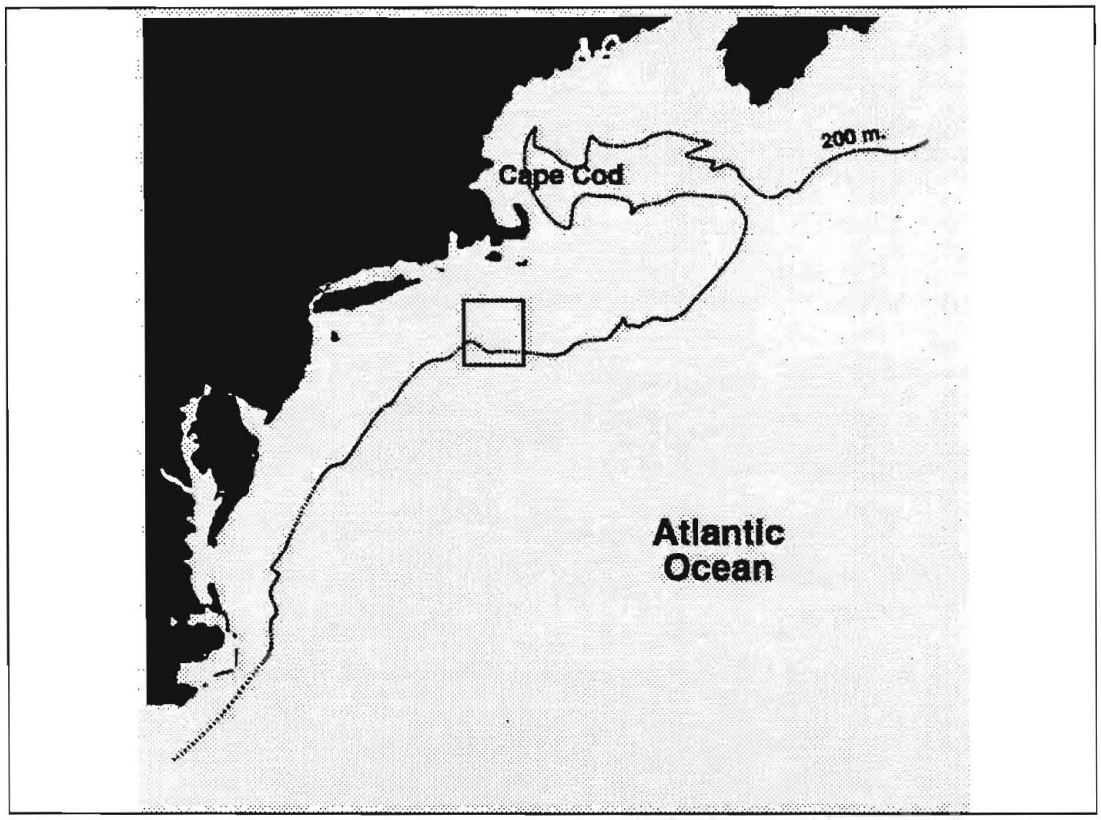

Figure 1. Proposed location of the Mid-Atlantic Bight Field Study as determined by Beardsley *et al.* (1994) (After Tchernia, 1962).

located at the continental shelf break south of Cape Cod. The tomography system will consist of a 224 Hz source, three 400 Hz transceivers and two vertical acoustic arrays composed of 15 hydrophones. The source and transceivers will transmit at an intensity level of 183 dB. Figure 2 shows the proposed experimental configuration in relation to the continental slope, shelf and oceanic frontal region. The characteristics of the sources and receivers are displayed in Table 1.

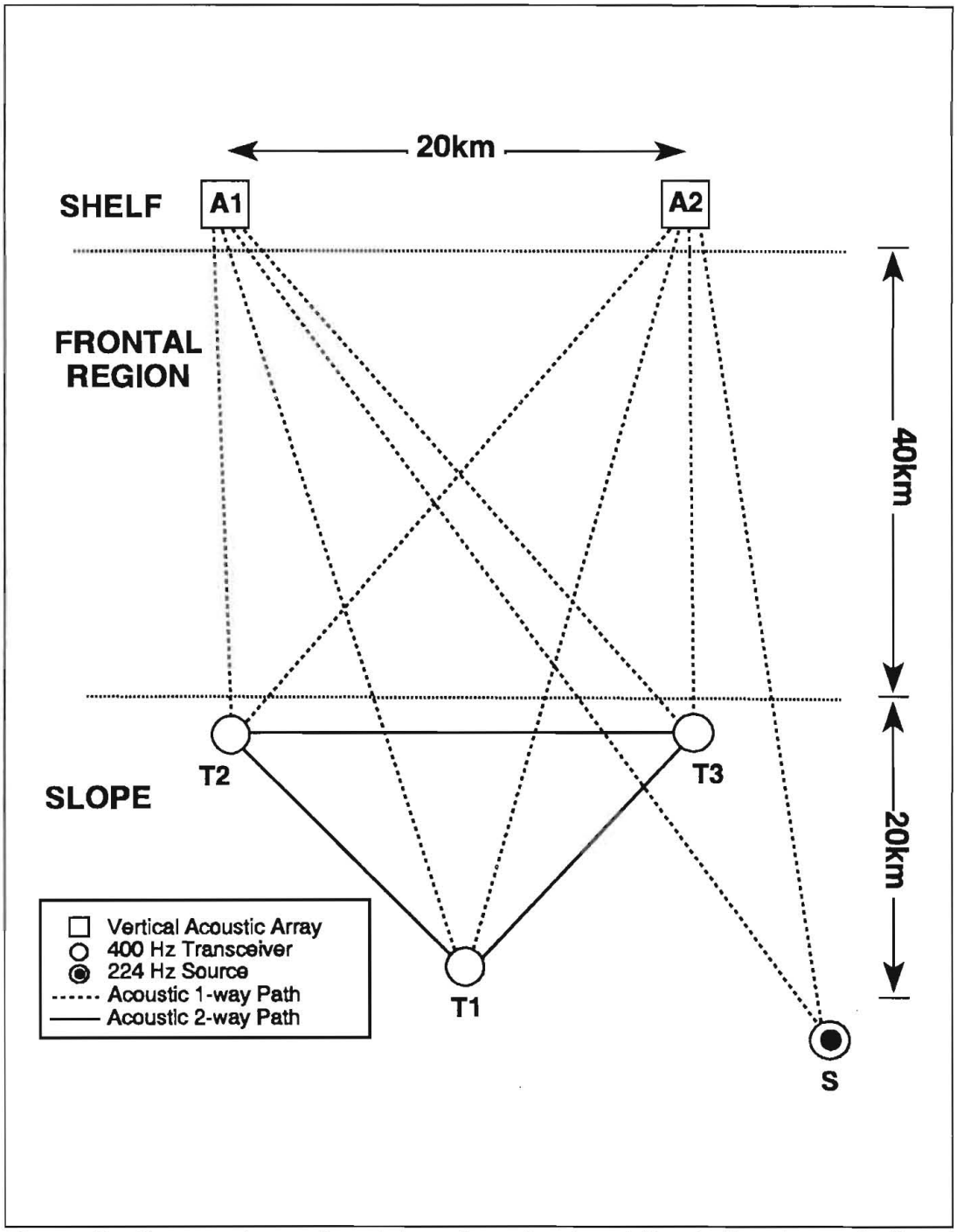

Figure 2. Proposed experimental configuration in relation to the slope, shelf and frontal region. Frontal region extends from a depth of 250 meters to a depth of 50 meters (After Beardsley *et al.*, 1994).

	Latitude (deg N)	Longitude (deg W)	Type	Frequency (Hz)	Bandwidth (Hz)
S	39.85	70.35	Source	224	16
T1	39.9	70.5	Transceiver	400	100
T2	40.1	70.6	Transceiver	400	100
T3	40.1	70.4	Transceiver	400	100
A1	40.5	70.6	Hydrophone Array	N/A	N/A
A2	40.5	70.4	Hydrophone Array	N/A	N/A

Table 1. Locations and Characteristics of Acoustic Elements.

This thesis will focus on a 400 Hz transceiver at the shelfbreak and a hydrophone array. The 400 Hz transceiver is mounted off a bottom depth of 250 meters on an oceanographic mooring. As will be presented in Chapter V, optimal results will be achieved if the transceiver is placed at a depth of 75 meters during the summer study and raised to a depth of 50 meters for the winter study. The hydrophone array is made up of 15 hydrophones mounted at a 3.5 meter incremental spacing on a vertical oceanographic mooring. This mooring will be placed on the continental shelf in 50 meters of water with hydrophones equally spaced throughout the entire water column with the bottom hydrophone placed at the ocean floor.

The scientific objectives of the Mid-Atlantic Bight Field Study can be summarized as follows (Beardsley *et al.*, 1994):

1. To obtain a high resolution description of the spatial and temporal evolution of the shelfbreak front, and clarify the mechanisms by which eddies are formed and detached.

2. To determine the mean and seasonally varying circulation of the adjacent slope water, and characterize the mesoscale fluctuation in relation to shelfbreak processes.

3. To determine the effects of basic mean shelfbreak frontal thermal structure on the propagation of sound from the continental slope to the continental shelf.

4. To relate the temporal and spatial variability of acoustic propagation from the continental slope to the continental shelf with the associated variability of the shelfbreak front.

5. To make fully three-dimensional tomographic images of the region of the shelfbreak front for use in physical oceanographic studies.

C. THESIS OBJECTIVES AND APPROACHES

The basic objectives of this thesis are broken into two distinct areas. The first is to study the oceanographic, geophysical and climatological conditions of the Middle Atlantic Bight to gain a better understanding of the environment. This is achieved through a literature search and personal contacts with various scientists.

The second objective is to address the tomography forward problem by examining the expected multipath arrival structure of the 400 Hz signal at the hydrophone array. The approach used to achieve this second objective is to run the ray tracing program HARPO (Hamiltonian Acoustic Raytracing Program for the Ocean) upgraded by Chiu *et al.* (1994) with simulated conditions anticipated during the actual testing of the Middle Atlantic Bight. The environmental information gathered provided the basis for building a mathematical model ocean used by HARPO. Use of actual temperatures, salinities and depths for computation of the sound speed fields will permit the modeled ocean to more closely approximate actual conditions than might otherwise be possible.

HARPO was used to trace a range of acoustic rays from a source to the receiving array. Ray traces were examined and used to compute the signal-to-noise ratio for various angles utilizing the transmission loss calculated for each ray. Eigenrays were determined and used to propose the depth of the tomographic sources. Additionally, the eigenrays were used to examine the ray path and arrival structures through analysis of arrival depths, times, angles and amplitudes. The resolvability of individual eigenray arrivals at the receiver was examined utilizing arrival times and a combination of arrival times and angles. Time analysis considered the hydrophone receivers as independent omni-directional receivers. Time and angle analysis considered the entire receiver array as a plane wave beamformer.

D. THESIS OUTLINE

The remainder of this thesis consists of five chapters. Chapter II describes the physical oceanography of the Middle Atlantic Bight including water masses, the oceanic front and Gulf Stream rings. Also included are discussions of the geologic structure and climatology of the test region.

Chapter III describes the acoustic properties of the Middle Atlantic Bight. Transmission loss comprised of absorption, bottom loss, surface loss, spreading and refraction as well as noise levels are explored. The calculation of the signal-to-noise ratio using source level, transmission loss, noise level and signal processing gains is conducted.

Chapter IV gives a brief review of ray theory and the ray tracing program HARPO. This discussion presents the basics of ray theory and the modeling of the physical environment of the Middle Atlantic Bight for input to HARPO.

Chapter V presents ray tracing results and eigenray development used to determine the optimal source depth and receiver hydrophone spacing, examine ray path and arrival structures and analyze resolvability concerns.

Chapter VI presents the conclusion of this study.

II. PHYSICAL OCEANOGRAPHY

A. INTRODUCTION

The dominant feature of the Middle Atlantic Region off the coast of the United States is the Middle Atlantic Bight. The Middle Atlantic Bight underlies the coastal plain, continental shelf and upper part of the continental slope of the Middle Atlantic United States. This region extends more than 500 kilometers subparallel with the shoreline between Cape Cod and Cape Hatteras. The seaward border of the Middle Atlantic Bight is a ridge of igneous basement or Mesozoic sedimentary rock that underlies the present upper continental slope. The Bight is at its widest off the coast of New Jersey and New York where it extends approximately 200 kilometers from the shoreline. (Poag, 1979)

The geographical location of the Middle Atlantic Bight lends itself to a complex oceanographic structure. With a maximum depth of approximately 200 meters on its seaward border and a depth of less than 50 meters over most of the bight, this region is considered a shallow coastal water area. This physical feature, coupled with the proximity of the Gulf Stream, generates many characteristics unique to the Middle Atlantic Bight.

The Mid-Atlantic Bight Field Study will be conducted in the northern portion of the region. The emphasis of this chapter will be on the oceanographic conditions expected to exist in the test area during the proposed time frame of the experiments (February and July).

B. WATER MASSES

The water masses of the Middle Atlantic Bight are characterized by many complex, but well-defined features (Figure 3).

The continental shelf is covered by waters of the coastal water band. This zone extends from the coastline to the 200 meter isobath (Von Arx, 1962). The movements of these waters are influenced by the tides and local coastal winds

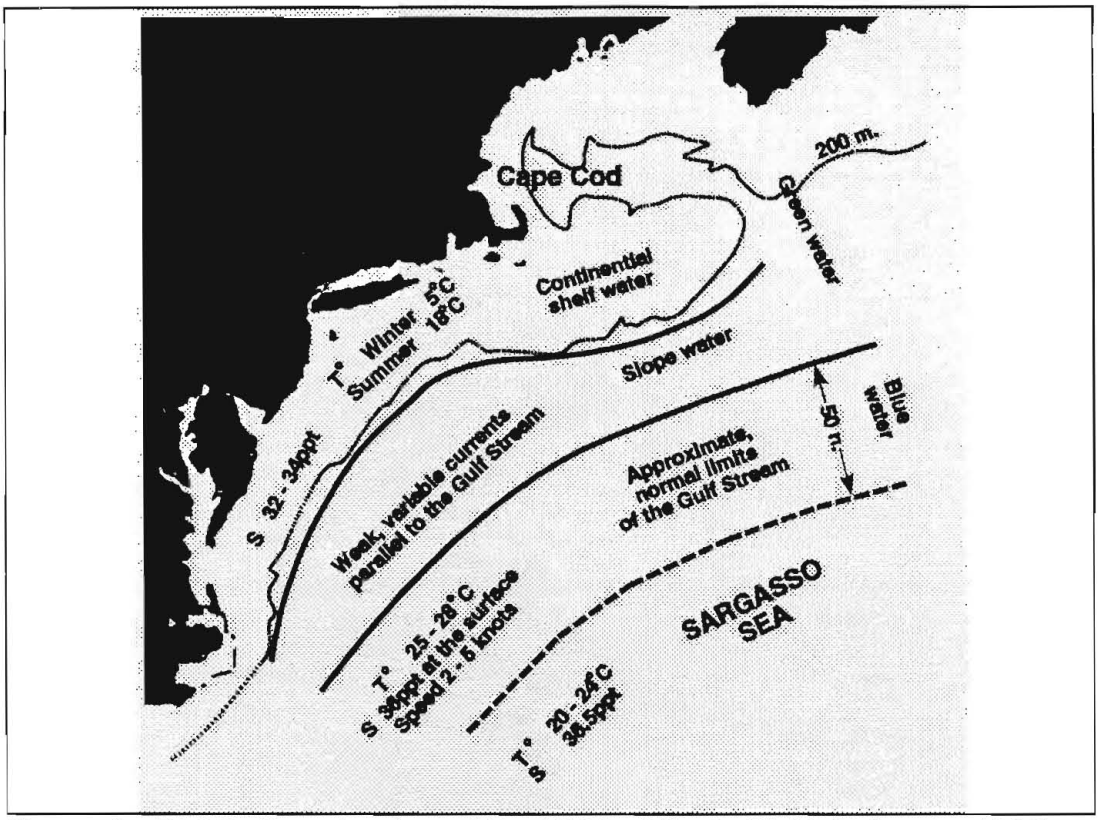

Figure 3. Distribution of waters of the Middle Atlantic Bight (Tchernia, 1962).

(Tchernia, 1980). Currents on the continental shelf have a systematic motion which is weak when compared with the flow in the rotary tides (Von Arx, 1962). Water characteristics are influenced by fresh water discharge from rivers and ground water, local precipitation and local plant life and vary considerably with the seasons and location. Sea water temperatures are approximately 5°C in the winter and 18°C in the summer, while the salinities range from 32 to 34 ppt year-round (Tchernia, 1962).

Between the shoulder of the continental shelf and the western edge of the Gulf Stream is a region called slope water. Currents in this region are weak in comparison with the tidal currents on the continental shelf and the flow of the Gulf Stream. Currents are often variable in speed from practically nil to 5 or 6 knots and tend to parallel the Gulf Stream (Tchernia, 1962). Temperatures and salinities

increase from the edge of the coastal water band towards the western edge of the Gulf Stream. At the eastern edge of the slope water, sea water temperatures range from 25 to 28°C and salinities are 35.5 to 36 ppt (Tchernia, 1962). Another feature of the slope water is the change in water color from the green coastal waters to the blue water of the Gulf Stream.

The transition of the coastal waters of the continental shelf to the slope waters is marked by the presence of a moderate strength oceanic front. Although the position of the front varies somewhat with the season and atmospheric conditions, the main axis of the front is found where the 18°C isotherm cuts the 200 meter isobath (Tchernia, 1962). The front is characterized by temperature differences of up to 5°C per 50 kilometers and is the strongest during the spring and summer (NAVOCEANO, 1984). As with most oceanic fronts, the surface aspects of the front passing through the Middle Atlantic Bight are often difficult to pinpoint due to turbulence and surface mixing. Accurate placement of the front's position can be determined by subsurface conditions.

C. GULF STREAM RINGS

The Gulf Stream system is composed of complex flows, eddies and meanders. In 1970, the formation of a cold or cyclonic eddy from a meander of the Gulf Stream was observed in "Operation Cabot" (Pickard and Emery, 1982). The name Gulf Stream Ring was suggested for these features which entrap colder slope water in the Sargasso Sea. Similarly, meanders may form on the north side of the Gulf Stream resulting in a warm water ring of Sargasso Sea water in the cooler slope water. The meanders in the Gulf Stream degenerate into the warm or cold water rings in much the same manner as oxbow lakes form from meandering rivers (Von Arx, 1962). The meanders begin forming loops which become longer and narrower, eventually becoming a self contained loop. Once formed the ring will completely separate from the Gulf Stream. A warm water ring is the oceanic equivalent of an atmospheric high pressure system, i.e. an

anticyclone. For this reason, the sense of rotation of warm water rings is often referred to as anti-cyclonic (Pickard and Emery, 1982). Rotation moves in a clockwise direction in the northern hemisphere.

Gulf Stream rings are usually 150 to 300 kilometers in diameter and some 3000 meters in the vertical dimension and have lifetimes of up to 2 years. After formation, rings move a few kilometers a day and eventually merge back into the Gulf Stream (Pickard and Emery, 1982). At any time there may be at least three warm water rings north of the Gulf Stream (Pickard and Emery, 1982).

D. GEOLOGIC STRUCTURE

Until the late 1960's little was known about the geologic structure or the sea floor sediments in the Middle Atlantic Bight region. Early studies by Alexander in 1934, Shepard and Cohee in 1936 and Stetson in 1939 were primarily limited to the continental shelf. Major findings included that a majority of sediments on the Atlantic continental shelf consisted of iron-stained quartz sands and gravels commonly containing fossilized shells. (Frank and Friedman, 1973)

The first detailed study of geologic structure occurred in 1967, when a consortium of oil companies (Exxon, Chevron, Mobile and Gulf) conducted their Atlantic Slope Project. They drilled eight core holes at seven sites along the base of the continental slope adjacent to the Middle Atlantic Bight (Poag, 1979). Oil exploration in the 1970's continued to fuel the need for further geologic studies.

The U.S. Geological Survey conducted intensive surveys of the shallow subbottom strata to evaluate geologic hazards of petroleum development in 1974-75 (Knebel and Spiker, 1977). Additional regional surveys included the Continental Offshore Stratigraphic Test in 1975, Atlantic Margin Coring Project in 1976 and Deep Sea Drilling Project leg 44 in 1975 and leg 95 in 1983 (Libby-French, 1984)(Schlee, 1981)(Robb *et al.*, 1981)(Hathaway *et al.*, 1979).

During these surveys thousands of core samples were drilled and analyzed. Cores were taken from the continental shelf as well as sea floor locations on the

continental slope down to approximately 2500 meters below the ocean's surface. Sea floor sediments and sedimentary rocks of Late Jurassic through Pleistocene age were recovered, but Miocene and Pleistocene strata constitute the bulk of the cored sections (Hathaway *et al.*, 1979)(Libbey-French, 1984). These sedimentary layers cover the basement rocks of the coastal plain which are primarily composed of igneous and metamorphic rock (Poag, 1979).

Analysis on cores taken from the uppermost continental slope generally revealed a very smooth surface covered by a thin surface layer (generally less than 2 meters thick) of medium grained Holocene sediments. These were underlain by texturally diverse Pleistocene sediments primarily composed of silty clay, silty sand, clayey sand or sandy clay (Robb *et al.*, 1981)(Hathaway *et al.*, 1979)(Poag, 1979). The thickness of the Pleistocene deposits range from about 450 meters at the top of the slope to very thin over large areas of the lower slope (Robb *et al.*, 1981).

Analysis on cores taken from the continental shelf revealed nearly horizontal layers of Pleistocene and early Holocene silty clays covered by various thicknesses of Holocene sands from 1 to 20 meters in depth. Average thickness of the sands was 5 to 7 meters. The surface layers were predominantly medium to coarse grained sands with varying amounts of shell fragments (Knebel, 1977).

The effects of geological structure on determining bottom loss acoustic properties will be covered in Chapter III.

E. CLIMATOLOGY

The climatology of the Middle Atlantic Bight Trough has been recorded and studied in detail for many years. The principal factors for the region's climate are the proximity of the Gulf Stream and the presence of prevailing winds from the south or the west. These effects combined with the presence of cooler coastal waters produce a very complex water mass structure and drive nearly all of the climatological processes occurring in this region. Table 2 provides a

meteorological climate summary for the test area for the months of February and July. Data was averaged over 30 years from a continuous climatological record maintained by the U.S. National Climate Center and the Naval Oceanographic Command (NAVOCEANO, 1992).

As observed in Table 2, the natural seasonal variations occur in mean sea surface and air temperatures. Sea surface temperatures during February average 7.1°C and increase to 21.8°C in July. July air temperatures average 22.5°C while February air temperatures average 3.9°C. The winter air temperatures are typically colder than the corresponding sea surface temperatures indicating that heat transfer from the water to the air is a predominant feature in the area. Unlike the mean sea surface temperature, mean air temperature and mean wind speed, discussed later in this section, the mean relative humidity does not show a strong annual pattern but instead shows only a slight variation from a morning average value of 80% to an afternoon average of 60%.

One effect of the warm air and water systems located near the Gulf Stream regions is the abundant precipitation and cloud cover. Cloud cover is heavily concentrated in the frontal regions. Cloud cover can be expected throughout the year, existing 73.2% of the time in February and 82.9% of the time during July. Annual monthly precipitation averages 3 to 4.5 inches.

Table 2 also shows mean sea level pressures for the experiment site at 1018.2 millibars in February and 1016.0 millibars in July. Both of these pressures are above the worldwide mean of 1013 millibars (Fairbridge, 1967). Closely related to atmospheric pressure is storm activity, usually associated with low pressure centers. Therefore, the test site is an area which is usually void of major storm activity.

Additionally, pressure differences produce wind. The prevailing winds in February are west-north west at 15.7 knots while the prevailing winds in July are out of the south at 10.1 knots. A major concern in the execution of any operation at sea is the occurrence of winds and the wave activity caused by these winds.

	February	July
Air Temperature (°C)	3.9	22.5
Sea Temperature (°C)	7.1	21.8
Precipitation (inches)	3.4	4.4
Days with > 0.01 inch Precipitation	10	9
Days with > 0.5 inch Precipitation	2	3
Days with Fog	12	19
Sea Level Pressure (mb)	1018.2	1016.0
Relative Humidity @ 0700 (%)	78	83
Relative Humidity @ 1600 (%)	59	60
Prevailing Wind Direction	WNW	S
Wind Speed (knots)	15.7	10.1
Visibility < 5 miles (%)	31	36
Visibility < 3 miles (%)	22	21
Visibility < 1 mile (%)	8	5
Occurrence of Clear Skies (%)	26.8	17.1
Occurrence of Scattered Clouds (%)	17.3	25.8
Occurrence of Broken Clouds (%)	15.1	26.8
Occurrence of Overcast Skies (%)	40.8	30.3
Wave Height (m)	1.3	0.67

Table 2. Average Meteorological Conditions for Test Area (After NAVOCEANO, 1992).

Average wave height in February is 1.3 meters while 0.67 meter waves can be expected in July. The roughness of the sea surface can greatly effect the propagation of sound in the ocean. The effects of sea surface roughness on propagation of sound will be discussed in Chapter III.

In summary, the environmental conditions during the months of February and July should be acceptable for the conduct of an ocean acoustic tomography experiment. With temperate temperatures and average wave heights of less than 1 meter, the July conditions should prove more acceptable for the testing and more comfortable for the test team. Although the February conditions, cold with average wave heights of 1.3 meters, will be less than ideal, they should provide an acceptable environment for the positioning of the bottom moored sources and receivers and for safe navigation by vessels involved. Average wave heights and the infrequency of major storm activity should allow for several days of continuous experimentation without interruption.

III. ACOUSTIC EFFECTS

A. INTRODUCTION

The study of sound propagation in the ocean requires a knowledge of the properties of the ocean medium, its boundaries and their influence on sound propagation. There are many factors to consider in the ocean environment. Clay and Medwin (1977) and Kinsler *et al.* (1982) and others describe many of these factors in detail. This chapter examines these factors and their contribution to the signal-to-noise ratio of the acoustic signal.

B. TRANSMISSION LOSS

Transmission loss (TL) is the sum of all the factors which affect the changes in acoustic energy from a transmitted signal. Major environmental factors which lead to this loss include water volume absorption, bottom loss, surface loss and spreading effects.

1. Water Volume Absorption

Water volume absorption is the loss of acoustic energy as sound travels through the water due to a conversion into thermal energy. Absorption loss (TL_{abs}) can be calculated as

$$TL_{abs} = \alpha r \qquad (3.1)$$

where α is the absorption coefficient and r is the distance travelled by the ray path. For a 400 Hz source, α is approximately 1.6×10^{-5} dB/m (Kinsler *et al.*, 1982). Therefore, for a distance of 45 kilometers, T_{abs} is 0.72 dB.

2. Bottom Loss

Bottom loss is the loss of acoustic energy over the traveled path due to each interaction with the ocean bottom. When a sound beam strikes the ocean floor, some of the beam may be reflected back into the water while some may be transmitted into the bottom. The reflected beam will have less energy than the

incident beam. The loss is a combination of direct transmission of some of the acoustic energy into the bottom and the scattering of acoustic energy due to bottom interactions and bottom attenuation. The bottom loss is a function of the bottom reflection coefficient which is a ratio of the acoustic energy reflected to that which is incident on the bottom.

While the propagation of sound in a fluid is completely compressional in nature, the speed of sound in the sea floor sediments is due to both propagation of compression and shear waves (Kinsler *et al.*, 1982). Therefore, to accurately determine the sediment sound speed properties, the geological structure of the region must be considered. As discussed in Chapter II, the surface sediments found on the continental shelf are primarily medium to coarse grained sands. The shear velocity for these sands is 250 m/s (Clay and Medwin, 1977) and the compressional speed is 1800 m/s (Schlee, 1981). The density of the sand found on the continental shelf is 2030 kg/m^3 (Clay and Medwin, 1977). The silty clay which makes up the top layers of the sediments found on the continental slope has a density of 1420 kg/m^3, a shear velocity of approximately 287 m/s (Clay and Medwin, 1977) and a compressional speed of approximately 1550 m/s (Schlee, 1981). For the given fluid-solid interface, the compressional wave attenuation coefficient is approximately 0.1 dB/m while the shear wave attenuation coefficient is approximately 1 dB/m (Tindle and Zhang, 1992).

The plane wave bottom reflection coefficient ($\Re_{12}$) at the water-sea floor interface is a function of bottom type, acoustic frequency (ω) and the grazing angle (θ). It can be calculated as per Tindle and Zhang (1992) as:

$$\Re_{12}(k) = \frac{\gamma_1 P(k) - (\rho_1/\rho_2)\gamma_2}{\gamma_1 P(k) + (\rho_1/\rho_2)\gamma_2} \tag{3.2}$$

where

$$P(k) = \left(1 - \frac{2k^2}{\left(\frac{\omega}{c_{s2}} + i\alpha_{s2}\right)^2}\right)^2 + \frac{i4\eta_2\gamma_s k^2}{\left(\frac{\omega}{c_{s2}} + i\alpha_{s2}\right)^4} \tag{3.3}$$

$$k = \frac{\omega}{c_1}\cos\theta \tag{3.4}$$

$$\gamma_1 = \sqrt{\left(\frac{\omega}{c_1}\right)^2 - k^2} \tag{3.5}$$

$$\gamma_2 = \sqrt{\left(\frac{\omega}{c_{p2}} + i\alpha_{p2}\right)^2 - k^2} \tag{3.6}$$

$$\gamma_s = \sqrt{\left(\frac{\omega}{c_{s2}} + i\alpha_{s2}\right)^2 - k^2} \tag{3.7}$$

$$\eta_2 = \sqrt{k^2 - \left(\frac{\omega}{c_{p2}} + i\alpha_{p2}\right)^2} \tag{3.8}$$

where c_1 is the speed of sound in the water, c_{p2} is the compressional wave velocity in the bottom sediments, c_{s2} is the shear wave velocity in the sediments, ρ_1 is the

water density, ρ_2 is the density of the sediments, and α_{p2} and α_{s2} are, respectively, the attenuation coefficients of the compressional and shear waves in the sediments.

Figure 4 plots $\Re_{12}$ as a function of grazing angle over a range of $0° < \theta < 90°$ for the water-sediment interfaces on the continental shelf and the continental slope. It can be seen on the figure that $\Re_{12}$ for the continental shelf begins to drop rapidly at approximately 26°. This is defined as the critical angle at which compressional waves no longer propagate into the lower medium even though incident energy is still transmitted into shear. For grazing angles less than the

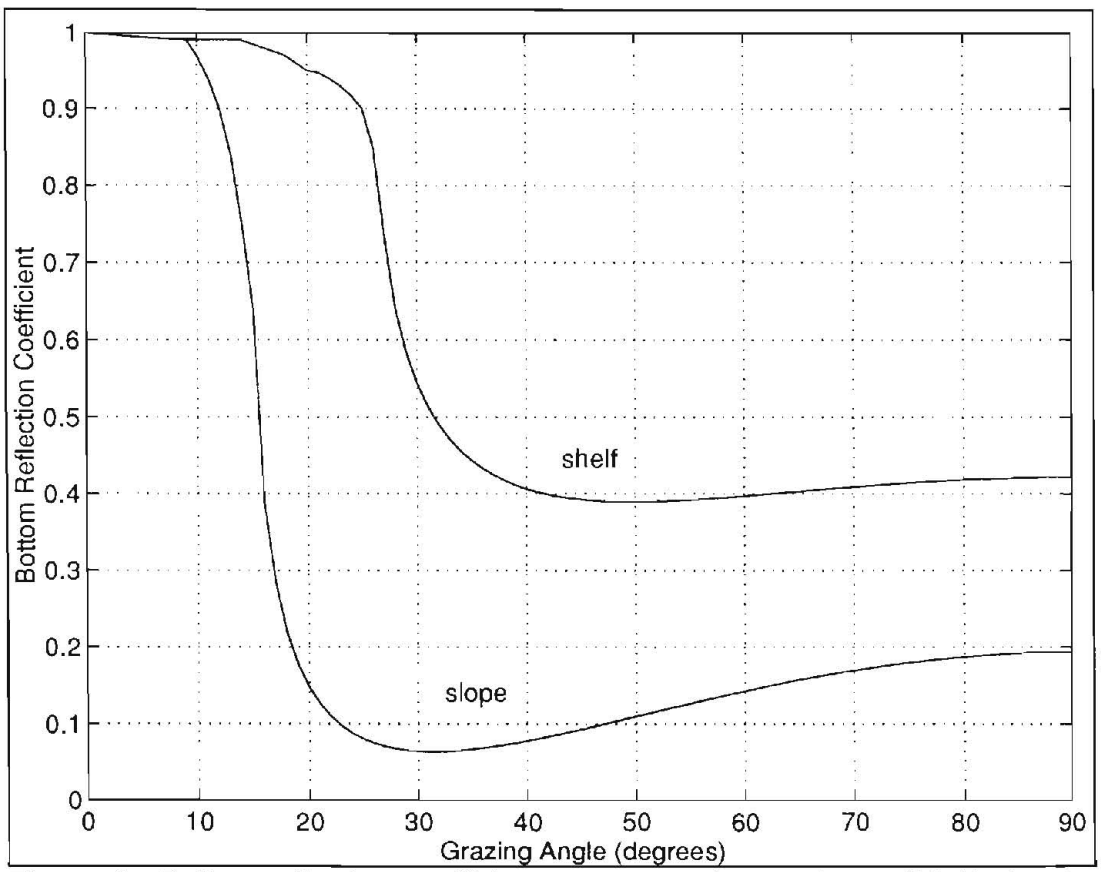

Figure 4. Bottom reflection coefficient versus grazing angle at 400 Hz for the Middle Atlantic Bight.

critical angle, energy is generally reflected with very little being transmitted into the sediments. Notice that on the continental slope the critical angle occurs at approximately 14°, due primarily to the slower compressional speeds of the sediments found in the slope's upper layers.

Bottom loss (BL) is a function of the bottom reflection coefficient and can be calculated as

$$BL = -20 \log (|\Re_{12}|) \tag{3.9}$$

Figure 5 plots the bottom loss as a function of grazing angle for the continental shelf and the continental slope. Note that on the shelf for grazing angles less than the critical angle of 26°, bottom loss is practically non-existent. However, for grazing angles greater than the critical angle bottom loss rises rapidly to at least 7 dB. It can be seen that the results on the slope are even more drastic than on the continental shelf. Bottom loss rises quickly to at least 15 dB after the critical angle of 14° is reached.

Acoustic rays traveling through the ocean can be approximated as the propagation of plane wave fronts through a medium. When considering the effects of attenuation in the bottom sediments it is noted that $| \Re_{12} | < 1$. Therefore, every interaction with the bottom will result in some bottom loss.

The total transmission loss due to bottom interaction is

$$TL_{bot} = N_{slope} BL_{slope} + N_{shelf} BL_{shelf} \tag{3.10}$$

where N is the number of bottom bounces the ray encounters. For the rays with launch angles greater than the critical angle of the shelf, the number of bottom bounces predicted by ray tracing analysis, as presented in Chapter V, exceeds 100 for both summer and winter conditions. This would lead to practically no energy at the receiver for those rays due solely to bottom interactions, given the 183 dB source level. Hence, rays that are launched at angles greater than 26° will be attenuated before reaching the receivers 45 kilometers downrange from the

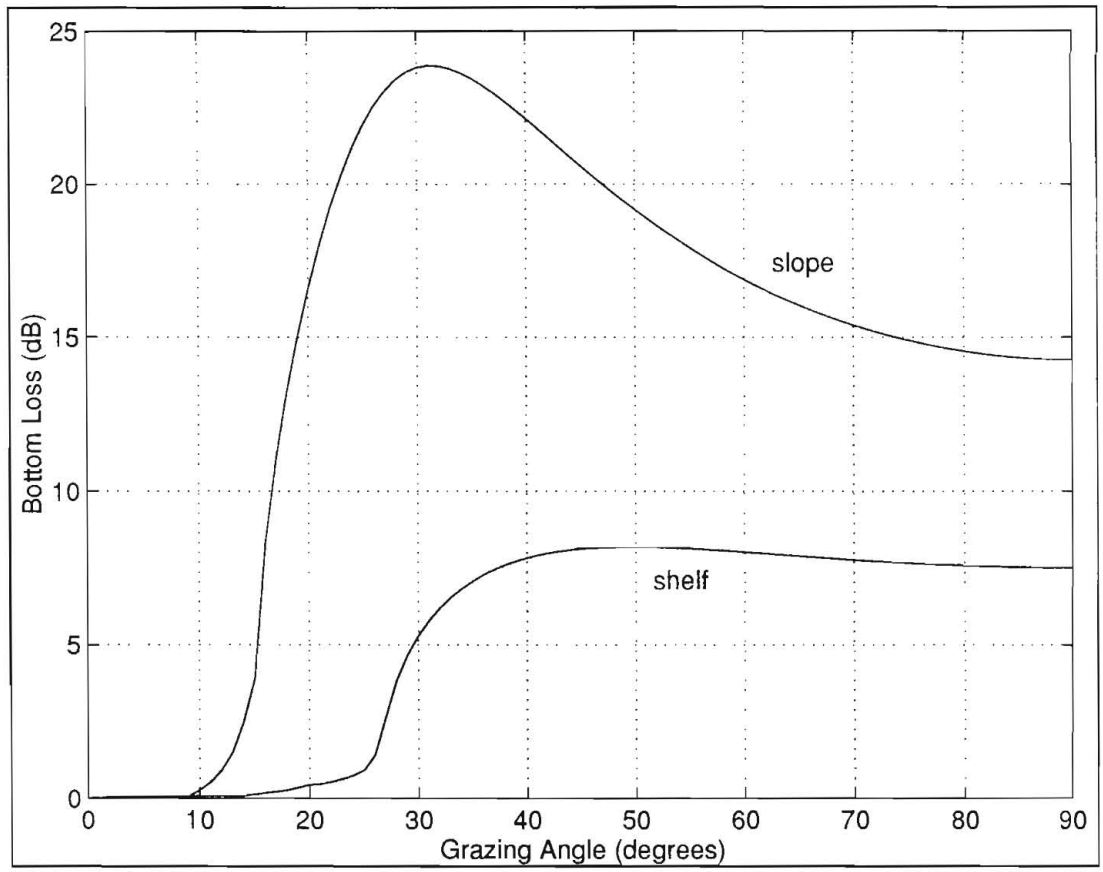

Figure 5. Bottom loss versus grazing angle at 400 Hz for the Middle Atlantic Bight.

source. For the Mid-Atlantic Bight Field Study, launch angles of interest will be those below the critical angle. For the source and receiver used in this study, ray tracing analysis predicts that no bottom bounces on the continental slope will occur for the launch angles of concern. However, bounces on the slope will occur for sources S1 and T1 so the slope curves and formulation are included for completeness.

To accurately calculate the total bottom loss, the number of bottom bounces that occur above and below the critical angle of the continental shelf must be considered. However, for this particular study ray tracing analysis predicted that no rays would arrive at angles greater than critical for the eigenrays of concern.

Tables 3 and 4 present the components contributing to the total bottom loss for various launch angles for summer and winter conditions.

launch angle	4°	5°	6°	7°	8°	9°	10°
N	7	12	20	28	36	43	67
BL	0.01	0.02	0.03	0.04	0.05	0.06	0.07
TL_{bot}	0.07	0.24	0.6	1.12	1.8	2.58	4.69

Table 3. Bottom loss components for various launch angles during summer conditions. Bottom loss measured in decibels.

launch angle	4°	5	6°	7°	8°	9°	10°
N	3	3	5	7	10	13	56
BL	0.01	0.02	0.03	0.04	0.05	0.06	0.07
TL_{bot}	0.03	0.06	0.15	0.28	0.5	0.78	3.92

Table 4. Bottom loss components for various launch angles during winter conditions. Bottom loss measured in decibels.

3. Surface Loss

Interaction of acoustic rays with the ocean surface results in the scattering of the sound from the reflected beam. Acoustic energy is lost with each ray reflection with the surface due to this scattering. These interactions are especially

important in shallow water applications. Surface loss is a function of the surface reflection coefficient which is the ratio of acoustic energy reflected to that which is incident upon the surface.

Assuming the sea surface has a Gaussian distribution, the surface reflection coefficient ($\Re_{surf}$) is a function of the wave number (k), root mean square wave roughness (σ) and the grazing angle (θ) and as per Clay and Medwin (1977) can be calculated as:

$$\Re_{surf} = e^{-2k^2\sigma^2\sin^2\theta} \tag{3.11}$$

Figure 6 plots $\Re_{surf}$ as a function of grazing angle over a range of $0° < \theta < 90°$ for sea state 1 (σ = 0.470 meters), sea state 3 (σ = 0.707 meters) and sea state 5 (σ = 2.05 meters) for the 400 Hz source signal.

Surface loss (SLOSS) is calculated directly from the surface reflection coefficient:

$$SLOSS = -20\log(|\Re_{surf}|) \tag{3.12}$$

Figure 7 plots the surface loss as a function of grazing angle for sea states 1, 3 and 5 for the 400 Hz source signal. It is observed that sea state has a dramatic effect on the amount of surface loss. For sea state 5 conditions, the surface loss is roughly an order of magnitude greater than for sea state 3. The total transmission loss due to surface interactions is

$$TL_{surf} = N(SLOSS) \tag{3.13}$$

where N is the number of surface bounces the ray encounters. Therefore, if heavy seas are encountered during the experiment, the signal losses due to surface interactions of high angle rays alone would be extremely large. Hence, except for very low angle rays, signals generated in high seas would be completely attenuated prior to reaching the receivers 45 kilometers downrange from the

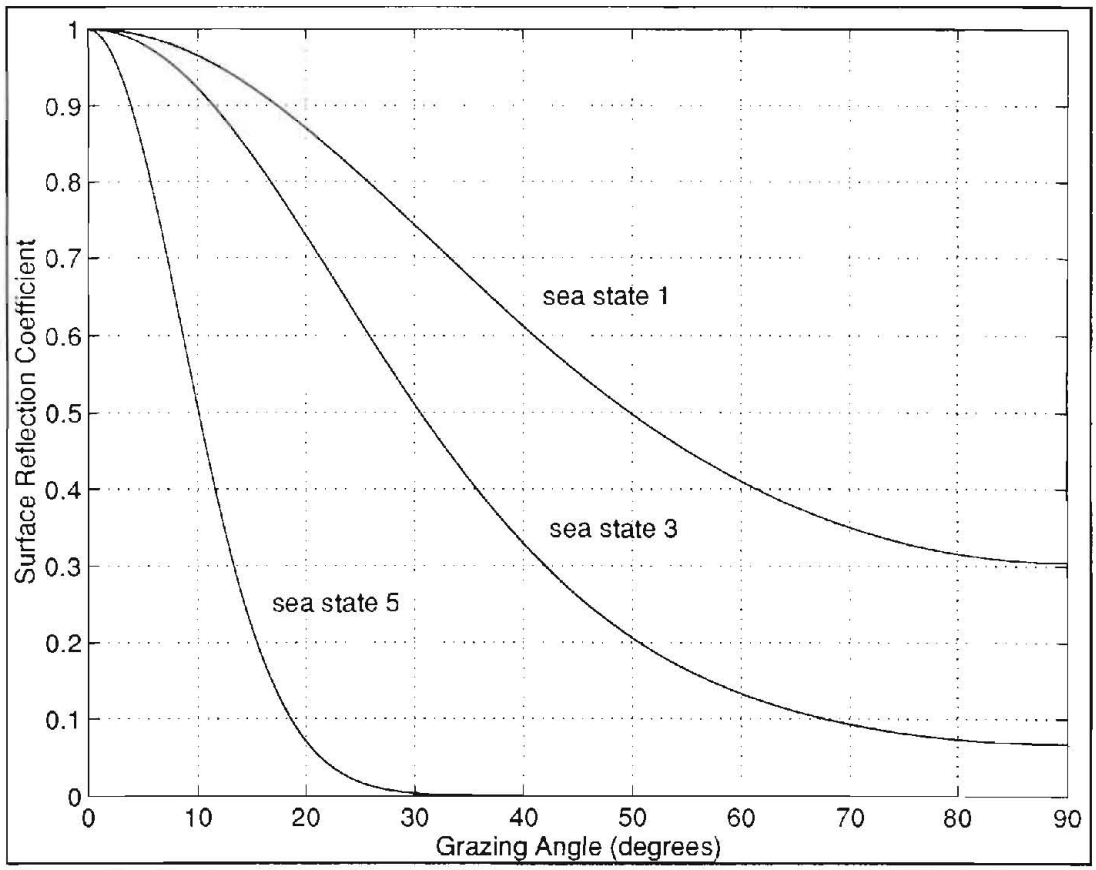

Figure 6. Surface reflection coefficient versus grazing angle at 400 Hz for sea states 1, 3 and 5.

source. However, for calm seas of sea state 3 or below the surface loss averages 1 dB for grazing angles less than the critical angle. Thus sea state may have a significant effect on the experiment results.

Tables 5 and 6 show the components contributing to the total surface loss for various launch angles expected during summer (sea state 1) and winter (sea state 3) conditions where the SLOSS provided in the tables is the average SLOSS encountered by all surface interactions from launch to arrival for the given launch angle.

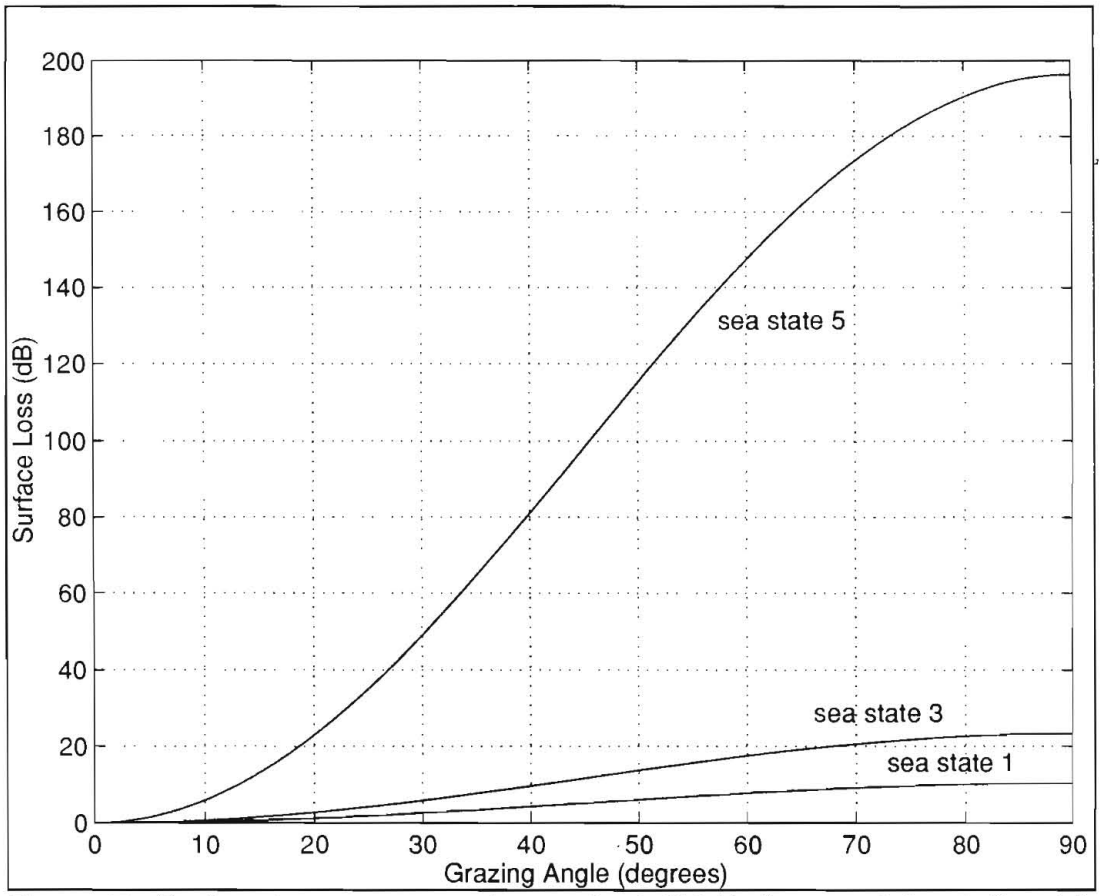

Figure 7. Surface loss versus grazing angle at 400 Hz for sea states 1, 3 and 5.

launch angle	4°	5°	6°	7°	8°	9°	10°
N	0	0	0	0	0	20	52
SLOSS	-	-	-	-	-	0.5	1
TL_{surf}	0	0	0	0	0	10	52

Table 5. Surface loss components for various launch angles during summer conditions at sea state 1. Surface loss measured in decibels.

launch angle	4°	5°	6°	7°	8°	9°	10°
N	28	29	30	31	31	34	57
SLOSS	0.2	0.25	0.8	1.5	2	3	5
TL_{surf}	5.6	7.25	24	46.5	62	102	285

Table 6. Surface loss components for various launch angles during winter conditions at sea state 3. Surface loss measured in decibels.

4. Spreading

Spreading transmission loss (TL_{spread}) is the loss over a traveled path from spatial variations in sound speed and properties of the waveguide. TL_{spread} occurs from the focusing and defocusing of adjacent rays as they travel away from a small spherical source and as per Clay and Medwin (1977) can be calculated as

$$TL_{spread} = 10 \log \frac{rhc_o \cos\theta}{(\Delta\theta) c \cos\theta_o} \qquad (3.14)$$

where r is the range between the source and receiver, h is the ray tube cross sectional distance at the receiver, c_o is the speed of sound at the source, c is the speed of sound at the receiver, θ_o is the launch angle of the ray, θ is the arrival angle of the ray and $\Delta\theta$ is the difference in launch angle between adjacently launched angles.

5. Summary

Transmission loss is the sum of all factors which affect the changes in acoustic energy from a transmitted signal. Tables 7 and 8 present the transmission losses expected during the summer and winter periods for the Middle Atlantic Bight. It is noted that transmission loss increases with increased launch angle in all seasons due to greater numbers of interactions with the sea surface and bottom. Note that the transmission loss for summer rays launched at approximately 10.4° and winter rays at 8.8° is 183 dB. Since this intensity level is equal to that of the source, rays launched at angles greater than these will be attenuated prior to reaching the receiver in the given sea state conditions.

launch angle	4°	5°	6°	7°	8°	9°	10°
TL_{abs}	0.72	0.72	0.73	0.74	0.74	0.75	0.76
TL_{bot}	0.07	0.24	0.6	1.12	1.8	2.58	4.69
TL_{surf}	0	0	0	0	0	10	52
TL_{spread}	91.0	91.9	89.9	90.4	90.2	92.1	91.1
TL	91.79	92.86	91.23	92.26	92.74	105.43	148.55

Table 7. Transmission loss components measured in decibels for various launch angles during summer conditions at sea state 1.

launch angle	4°	5°	6°	7°	8°	9°	10°
TL_{abs}	0.72	0.72	0.73	0.73	0.74	0.74	0.75
TL_{bot}	0.03	0.06	0.15	0.28	0.5	0.78	3.92
TL_{surf}	5.6	7.25	24	46.5	62	102	285
TL_{spread}	85.9	86.6	85.7	86.1	86.8	85.5	87.1
TL	92.25	94.63	110.58	133.61	150.04	189.02	376.77

Table 8. Transmission loss components measured in decibels for various launch angles during winter conditions at sea state 3.

C. NOISE LEVEL

Noise is an ever-present phenomenon which must be considered in the propagation of sound. A received signal, after processing, must be at least as loud as the noise level to be useful. There are two basic types of noise which must be taken into account for any marine environment experiment: ambient noise and self noise.

Ambient noise is the noise existing in the environment in the absence of the receiving platform and target source. Major contributions to ambient noise are distant shipping traffic, ocean turbulence, sea state and biological noise from marine life. Biological noise is usually very small when compared to the other factors and will not be considered. The remaining parameters of ambient noise can be obtained from the Wenz Curves (Wenz, 1962). For a 400 Hz source signal the effects of ocean turbulence are negligible. The Wenz Curves contain plots of the ambient noise spectrum levels for high and low shipping density areas. The

Middle Atlantic Bight area can be expected to have high shipping traffic year-round. Therefore, the noise spectrum level (NSL) associated with shipping for a 400 Hz source is found to be 50 dB re 1 μPa/Hz$^{1/2}$. The noise level (NL) must be corrected to reflect the bandwidth (w) considerations

$$NL = NSL + 10 \log(w) \tag{3.15}$$

For the 100 Hz bandwidth of the 400 Hz source, NL_{ship} is raised to 70 dB re 1 μPa.

Sea state has a dramatic effect on the ambient noise level, increasing with increased wave height due to sea surface agitation and wind speed. For a sea state of 1 the noise spectrum level is 57 dB whereas for a sea states of 3 and 5 the noise spectrum level raises to 66 dB and 75 dB respectively. As with shipping noise, these values must be corrected for the bandwidth resulting in 77 dB, 86 dB and 95 dB re 1 μPa respectively.

Self-noise is the noise created by the receiving platform which interferes with the received signal. The receiving platform currently planned for use in the Mid-Atlantic Bight Field Study is a single buoy system connected to the vertical hydrophone array. Self-noise will be negligible if a sole buoy system is used, however must be considered if a ship is scheduled to be used.

As noise is an intensity level the total noise level is calculated by a power summation of the individual noise components

$$NL = 10 \log(\sum 10^{NL_i/10}) \tag{3.16}$$

Use of the power summation results in sea state noise dominating all other forms of noise. For sea state 1 conditions typical of summer conditions, total noise level for a 400 Hz source with a 100 Hz bandwidth is 77.8 dB re 1 μPa. For sea state 3 conditions typical of winter conditions, total noise level for a 400 Hz source with a 100 Hz bandwidth is 86.1 dB re 1 μPa.

D. SIGNAL-TO-NOISE RATIO

Signal-to-noise ratio (SNR) is the ratio of the received signal to environmental noise level and is calculated as

$$SNR = SL - TL - NL + PCG + CAG \tag{3.17}$$

where SL is the source level. TL is the transmission loss and NL is the noise level as previously defined. PCG is the pulse compression gain and CAG is the coherent averaging gain. All components are measured in decibels referenced to 1 μPa at 1 meter. The source level to be used in the Mid-Atlantic Bight Field Study will be 183 dB transmitted at the center frequency of the moored sources. The gains are obtained through signal processing (Spindel, 1979) and are defined as

$$PCG = 10 \log (m\ sequence\ digits) \tag{3.18}$$

$$CAG = 10 \log (sequence\ repetitions) \tag{3.19}$$

The 400 Hz tomographic transceivers to be used in this experiment have a kernel m-sequence of 511 digits which results in a pulse compression gain of 27 dB. With 30 repetitions of the sequences, a coherent averaging gain of 15 dB is obtained.

Tables 9 and 10 tabulate the previously presented components of signal-to-noise ratio. As expected, the signal-to-noise ratio decreases with increased elevation angle due to larger amounts of transmission loss. As the transmission loss increases with larger angles, signal processing gains become increasingly important and may actually be required in order to discriminate the signal from the background noise.

launch angle	4°	5°	6°	7°	8°	9°	10°
SL	183	183	183	183	183	183	183
TL	91.79	92.86	91.23	92.26	92.74	105.43	148.55
NL	77.8	77.8	77.8	77.8	77.8	77.8	77.8
PCG	27	27	27	27	27	27	27
CAG	15	15	15	15	15	15	15
SNR	55.41	54.34	55.97	54.94	54.46	41.77	-1.35

Table 9. Signal-to-noise components measured in decibels for various launch angles during summer conditions at sea state 1.

launch angle	4°	5°	6°	7°	8°	9°	10°
SL	183	183	183	183	183	183	183
TL	92.25	94.63	110.58	133.61	150.04	189.02	376.77
NL	86.1	86.1	86.1	86.1	86.1	86.1	86.1
PCG	27	27	27	27	27	27	27
CAG	15	15	15	15	15	15	15
SNR	46.65	44.27	28.32	5.29	-11.14	-50.12	-237.87

Table 10. Signal-to-noise components measured in decibels for various launch angles during winter conditions at sea state 3.

IV. RAY THEORY ACOUSTICS

A. INTRODUCTION

Ray theory or geometrical acoustics is the study of sound behavior under the assumption that sound waves transversing a medium travel along geometric paths called rays. The refractive index of an inhomogeneous medium changes throughout thereby bending the acoustic ray path. An acoustic ray path will always bend toward the region of lower sound speed. Ray theory allows for a visual depiction of paths taken by sound energy and graphically illustrates the effects on each ray by various ocean parameters.

The general purpose underwater acoustic ray tracing program HARPO (Hamiltonian Acoustic Raytracing Program for the Ocean) is used in this thesis. This three dimensional ray tracing program uses continuous treatment of sound speeds and bathymetric structure thereby eliminating the problems of false caustics and discontinuous ray path properties (Jones *et al.*, 1986).

B. HAMILTONIAN RAY TRACING

Rays can be traced by integrating Hamilton's equations which are differential forms of Fermat's principle (Jones *et al.*, 1986). Hamilton's equations govern the changes of position and momentum in mechanical systems. In the high frequency limit, where sound waves behave like particles and travel along rays, Hamilton's equations are applicable to the propagation of sound (Lighthill, 1978). High frequency for use in the ray tracing method occurs when the source signal wavelength is much less than the water depth and much less than the distance separating the source and receiver (Miller, 1995). Even in lower frequency situations, where ray theory does not strictly apply, Hamilton's equations and acoustic ray paths often provide valuable insight to sound propagation in the ocean (Jones *et al.*, 1986).

In two dimensions, Hamilton's equations have the general form:

$$\frac{dq_i}{dt} = \frac{\partial H}{\partial p_i} \qquad i = 1,2 \tag{4.1}$$

$$\frac{dp_i}{dt} = -\frac{\partial H}{\partial q_i} \qquad i = 1,2$$

where $H(p_1,p_2;q_1,q_2)$ is the Hamiltonian function describing the total energy of a system in terms of a generalized coordinate system q_i and momenta p_i (Fowles, 1986). For acoustic applications, p_i are proportional to the wave number components k_i and q_i are the rectangular coordinates x_i of a point on the ray path. HARPO uses a spherical polar coordinate system. Solutions to Equation 4.1 are obtained by choosing initial values for the quantities k_i and x_i and integrating this system of four differential equations. For sound propagation in the ocean, the Hamiltonian is defined as

$$H(r,z;k_r,k_z) = \omega^2 - c^2(r,z)[k_r^2 + k_z^2] = 0 \tag{4.2}$$

where ω is the angular wave frequency and c is the sound speed field, r is range, z is depth, k_r is the horizontal wave number and k_z is the vertical wave number. (Jones *et al.*, 1986)(Smith, 1995) As can be seen by Equation 4.2, the Hamiltonian is defined as zero along the ray path.

C. HARPO OVERVIEW

HARPO is a computer algorithm that numerically integrates Hamilton's equations to trace three dimensional acoustic ray paths through a model ocean. The model ocean is input by the user and consists of a continuous three dimensional representation of the sound speed field and continuous two dimensional representations of upper and lower reflecting surfaces. The upper and lower reflecting surfaces are chosen to be the ocean surface and ocean bottom respectively.

Chiu *et al.* (1994) created a computer subroutine external to HARPO called DINP which allows for the input of discrete values for the sound speed and bathymetry fields. The discrete data points are made continuous through the use of empirical orthogonal functions and splines. HARPO uses these continuous fields as its input for computation of the numerical integrations to solve Hamilton's equations.

The model ocean input to HARPO must be deterministic, not random, as HARPO's computations apply no corrections for diffraction or partial reflections. Realistic ocean models must be input, as HARPO has no means to verify if ocean models are physically practical and will allow inconsistent models to exist. Furthermore, HARPO does not compute acoustic amplitude or eigenrays. These calculations are made by external programs using the HARPO output files DOUTP and RAYSET (Chiu *et al.*, 1994). For a complete description of HARPO including the mathematics and computer coding, the reader is referred to the HARPO documentation by Jones *et al.* (1986).

D. MODELING THE ACOUSTIC ENVIRONMENT

The precision with which HARPO calculates ray paths is dependent on the accuracy with which the ocean test area is described by the input models. Chapter II described the oceanographic environment of the Middle Atlantic Bight. Modeling this environment for acoustic ray analysis was accomplished by selecting computer routines and environmental data for acceptable mathematical descriptions of the sound speed field and bathymetry.

The bathymetry input to HARPO is shown in Figure 8. Bathymetry data for the Middle Atlantic Bight region was obtained from the World Bathymetry Data Base DBDB-5. This data base consists of bathymetric/tomographic data for every 5 minutes (1/12°) of latitude and longitude for the entire earth. Data is rounded to the nearest meter.

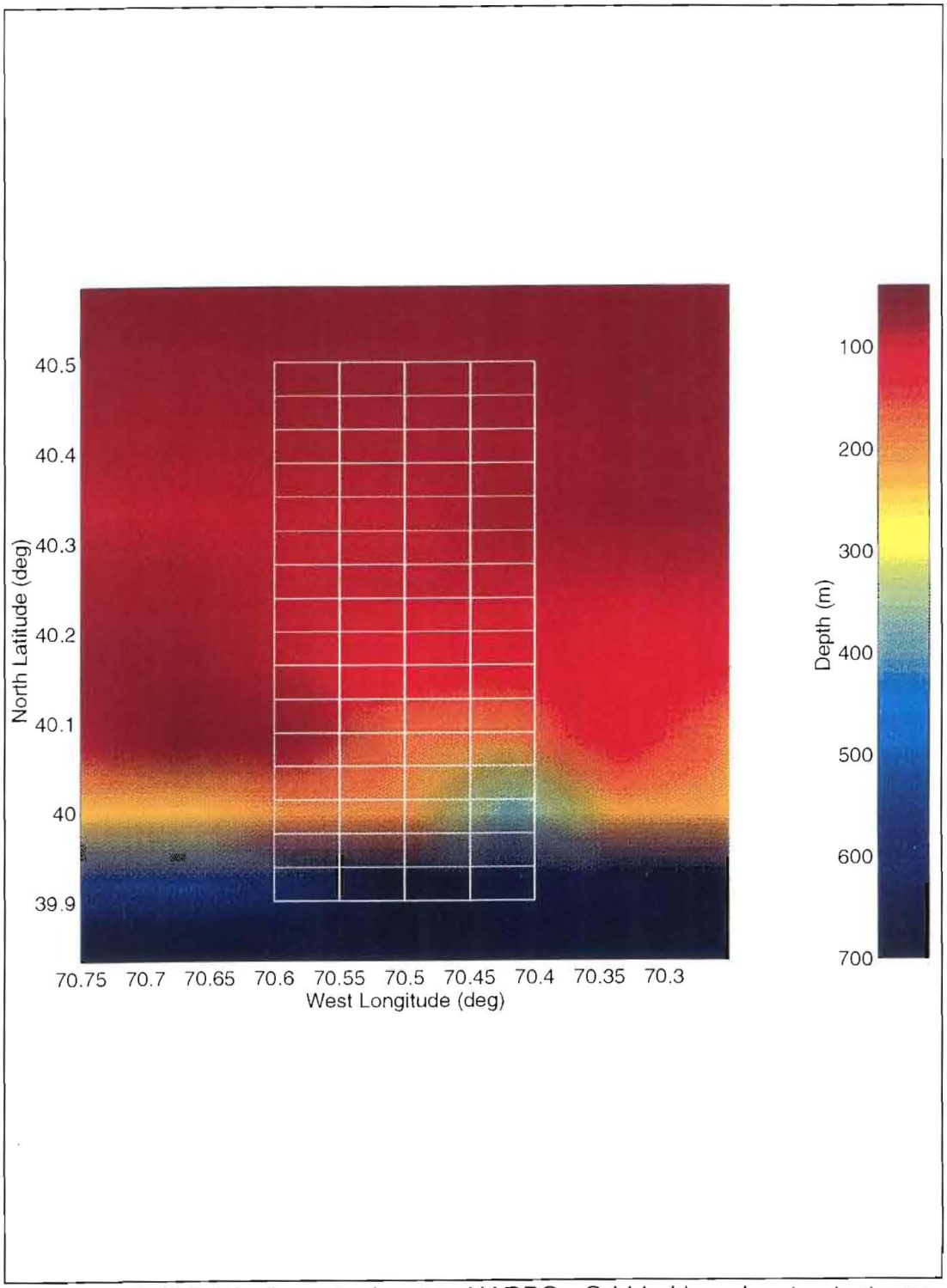

Figure 8. DBDB-5 bathymetry input to HARPO. Gridded box denotes test area.

The test area was outlined by the 60 km x 20 km rectangular box and gridded into 17 subdivisions along the long side and five along the short side creating 80 3.75 km x 5 km subdivisions. The bottom depths at each grid intersection were manually read off of the DBDB-5 plot, splined and input to HARPO using the DINP subroutine.

The input sound speed profiles for HARPO were created as an iterative process. Sound speeds for each grid intersection were calculated using temperature and salinity data obtained by Woods Hole Oceanographic Institution. Data was collected for both summer and winter conditions at 2 meter depth increments throughout the test area. Sound speed data points were obtained for every 2 meters of depth at each of the grid intersections. (These sound speed data points and a refined environmental model developed by Chiu based on the Woods Hole data were submitted by Beardsley *et al.* (1994).) The sound speed data points were splined together using linear interpolation to create continuous sound speed profiles to the deepest bottom depths. Additionally, early runs of HARPO on the raw data resulted in the tracing of non-realistic rays and ray entrapment due to fine structure perturbations. These rays are extremely sensitive to initial and environmental conditions due to the chaotic nature of ray trajectories in range-dependent environments (Smith, 1992). This established a requirement to filter the sound speed profiles prior to input to HARPO to reduce this sensitivity. Filtered sound speed profiles to depths of 250 meters, representative of five select locations in the Middle Atlantic Bight test area, for summer and winter conditions are shown in Figure 9. The test area locations illustrated in Figure 9 are the seaward edge (SSP1), one quarter distance from the seaward edge (SSP2), the midpoint (SSP3), one quarter distance from the shoreward edge (SSP4) and the shoreward edge (SSP5). Continuous three-dimensional sound speed fields were developed by combining the sound speed profiles with the bathymetric field, thereby generating sound speed as a function of depth, latitude and longitude.

Figure 10 presents continuous sound speed fields for summer and winter conditions for a vertical slice running down the center of the test region.

The sea surface was modeled as a flat sphere concentric with the earth with no perturbations. No bottom perturbations were input into the model ocean.

The environmental model created placed a 40 kilometer oceanic front between the transceiver source and the receiver array. Table 1 and Figure 2 detail source and receiver positions. In the simulations performed, the transceiver source was placed near the shelfbreak in 250 meters of water at a depth of 75 meters for summer conditions and 50 meters for winter conditions. The receiver array was placed in 50 meters of water at a distance of 45 kilometers from the transceiver.

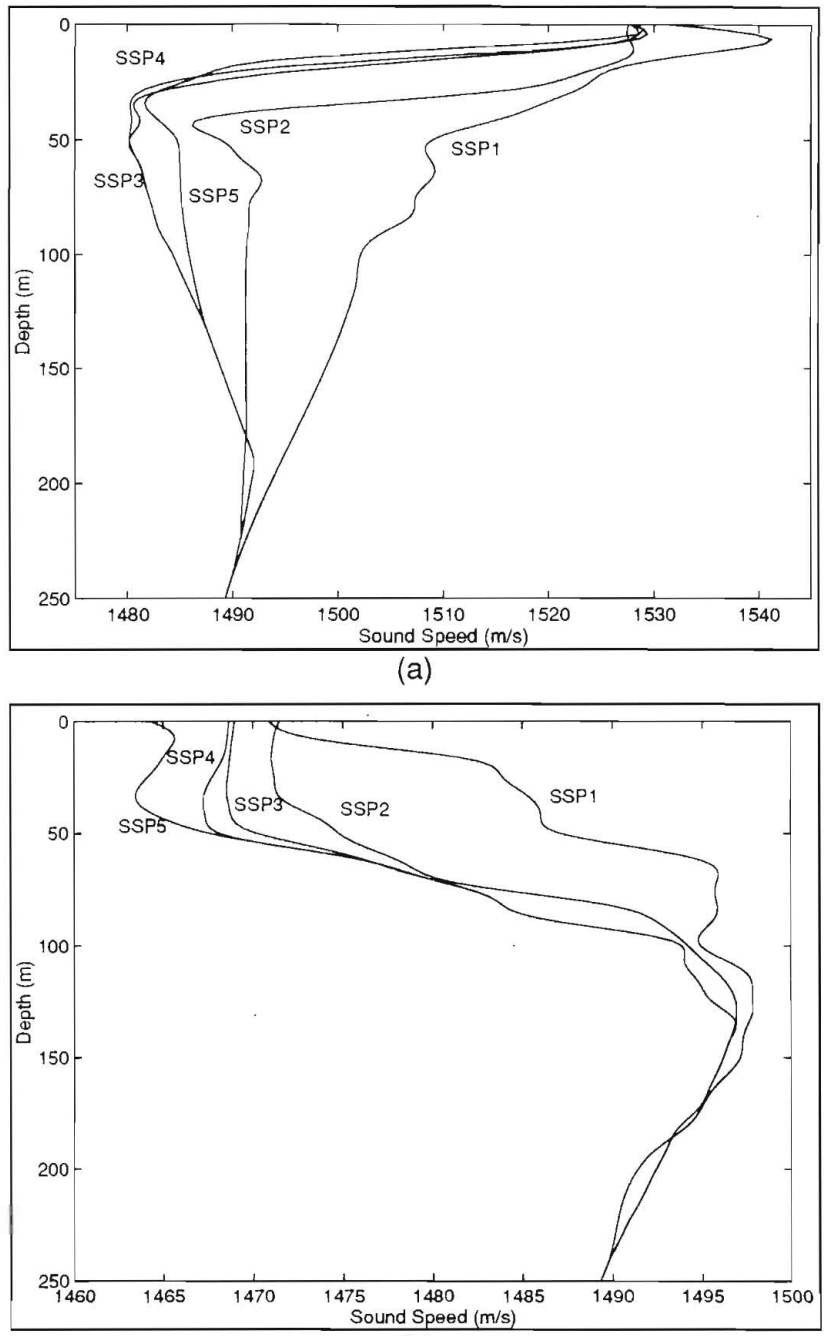

Figure 9. Filtered sound speed profiles representative of select locations for (a) summer conditions and (b) winter conditions.

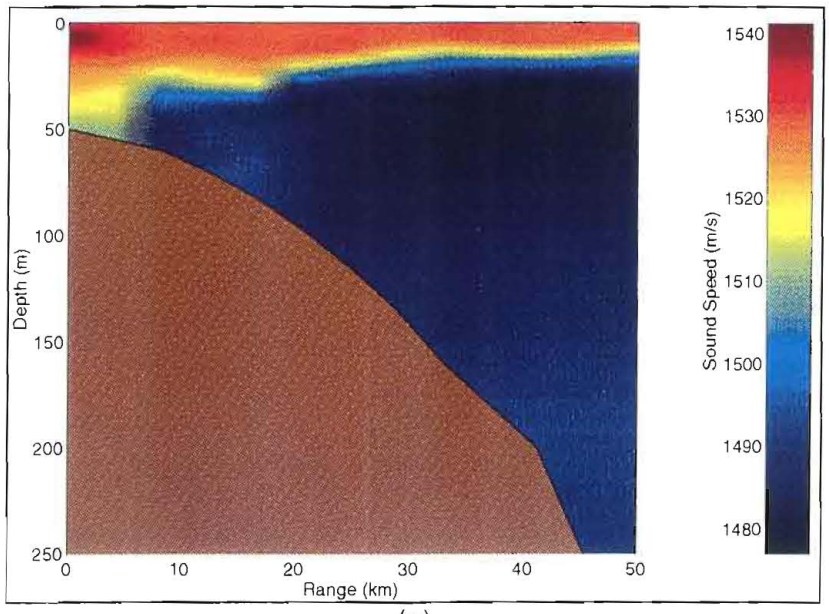

(a)

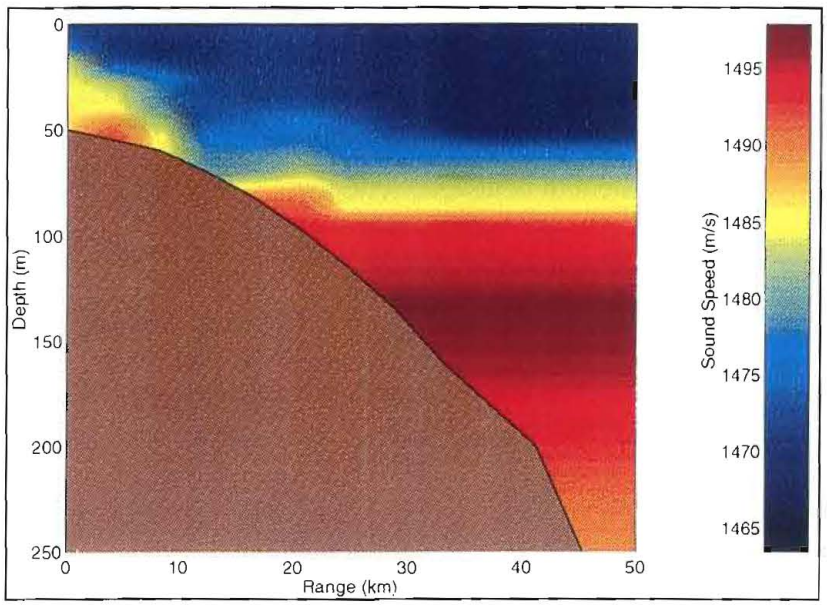

(b)

Figure 10. Continuous sound speed fields for (a) summer conditions and (b) winter conditions.

V. ARRIVAL STRUCTURE SIMULATION AND ANALYSIS

A. INTRODUCTION

To simulate the propagation of the 400 Hz tomographic signal from the source through the front to the vertical hydrophone array, rays were traced using HARPO with inputs as described in Chapter IV. HARPO results were input into a MATLAB™ program *rbreak.m* which processes the results to find eigenrays between a source and receiver pair over a given range. Arrival time and angle, path distance, ray amplitude and phase are computed for each eigenray.

B. SOURCE DEPTH DETERMINATION

In order to determine the best depth for the transceiver sources, HARPO was used to perform ray traces for launch angles between -25.0° to 25.0° at 0.1° increments. The initial simulations were conducted by placing a source in the shallow waters of the continental shelf at the actual location of the receiver array. Through the principle of acoustic reciprocity, the locations of a source and receiver may be interchanged and the received signal will remain the same. While the simulations were conducted downslope, the actual experiments will be conducted upslope onto the continental shelf. The rays were traced from a mid-column source in 50 meters of water downslope over a range of 45 kilometers. *rbreak.m* was performed on these 501 ray traces for both summer and winter conditions. The actual source depth for each season was determined by choosing the depth through which the greatest number of eigenrays from the mid-column "source" passed. Additional consideration was given to the launch and arrival angles associated with the eigenrays. As discussed in Chapter III, high elevation angles are not likely to transit the entire 45 kilometers due to the high transmission loss associated with numerous boundary interactions. Furthermore, rather than progressing forward, high elevation angles tend to reflect back towards the source when striking the upward sloping ocean floor. Of the 501 rays used in these

simulations, 123 low angle eigenrays traveled through a depth of 75 meters for summer conditions, while 110 low angle eigenrays transversed through a depth of 50 meters for the winter simulation. These depths were thereby chosen as the actual source depths for the Mid-Atlantic Bight Field Study. Figures 11 and 12 provide plots showing the number of eigenrays with arrival angles for various depths used to determine the actual source depths.

C. RAY PATH STRUCTURE

To examine the effects of the environmental conditions on the structure and stability of the ray paths, ray traces were constructed for various launch angles using data obtained from the *rbreak.m* results. Figure 13 shows a ray launched at 4° for both summer and winter conditions. It is observed that under summer conditions, rays launched at shallow grazing angles are refracted bottom-reflected (RBR) as expected by the downward refracting sound speed profile (Figures 9a and 10a). Rays launched at shallow grazing angles under winter conditions are refracted surface-reflected (RSR) as expected with the upward refracting sound speed profile obtained from a cold surface layer (Figures 9b and 10b). As the launch angle becomes greater, ray traces for both seasons will tend to become completely surface-reflected bottom-reflected (SRBR). Additionally, the number of interactions with the bottom and surface increases with increased launch angle (Figure 14).

D. ARRIVAL STRUCTURE

The arrival structure can be studied by examining various plots made from the 501 rays traced between -25.0° to 25.0°. While information can be gained from all the rays traced, the most important information is obtained from the eigenrays, those rays which propagate from the source to a particular receiver. Conclusions on the feasibility of conducting this ocean acoustic tomography project can be based on the arrival times, depths and angles of eigenrays transversing the entire

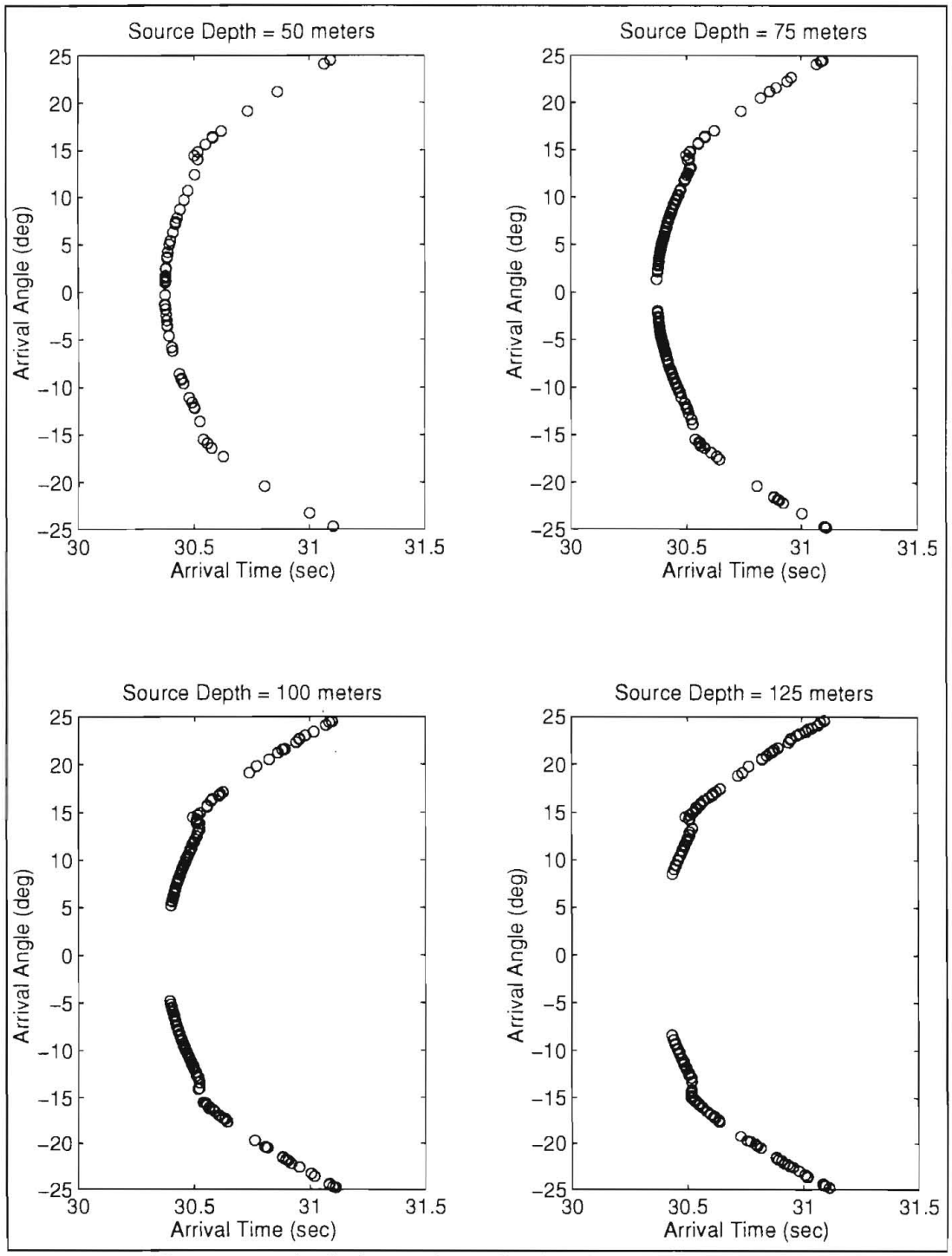

Figure 11. Eigenray arrivals for various depths during summer conditions used to determine source depth.

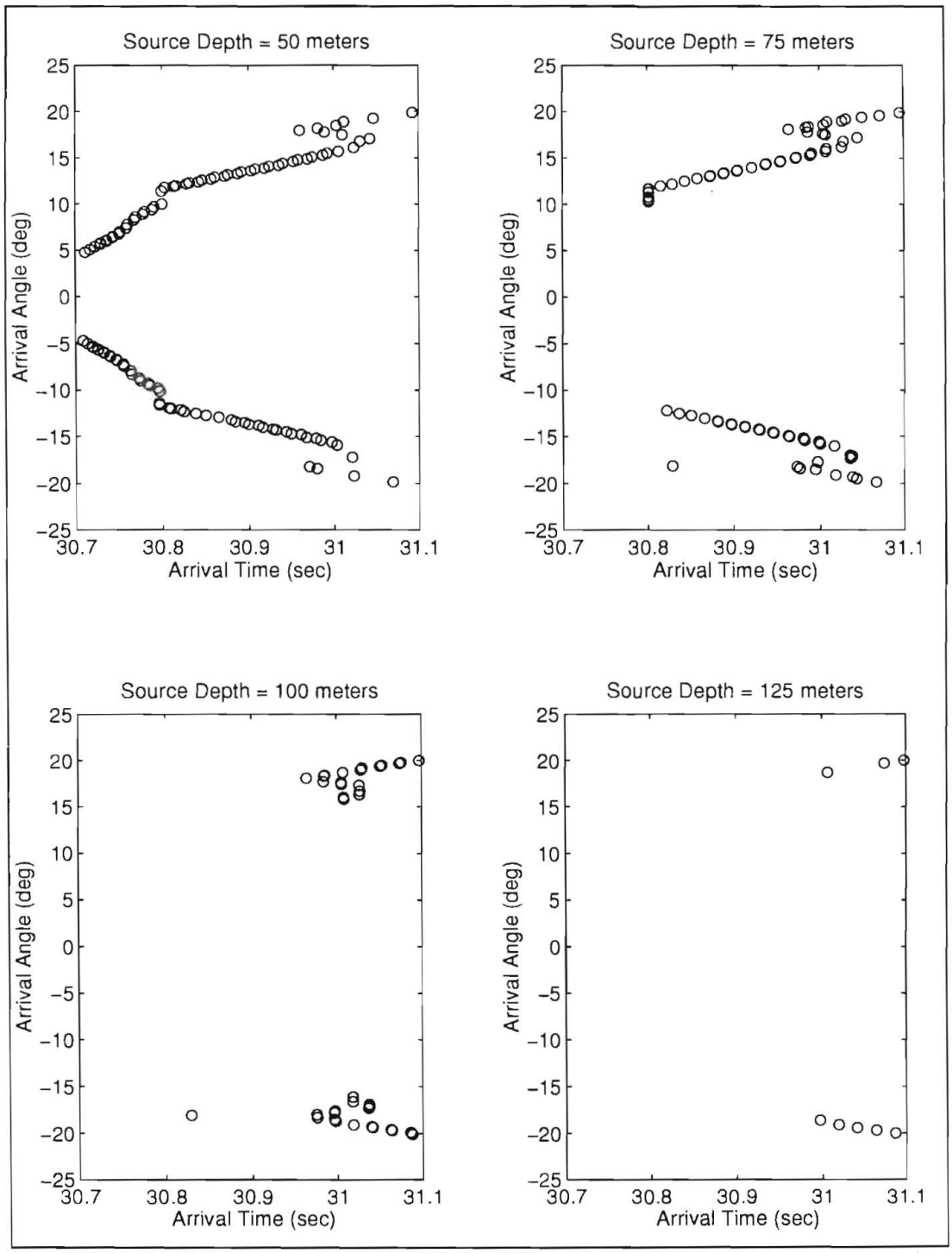

Figure 12. Eigenray arrivals for various depths during winter conditions used to determine source depth.

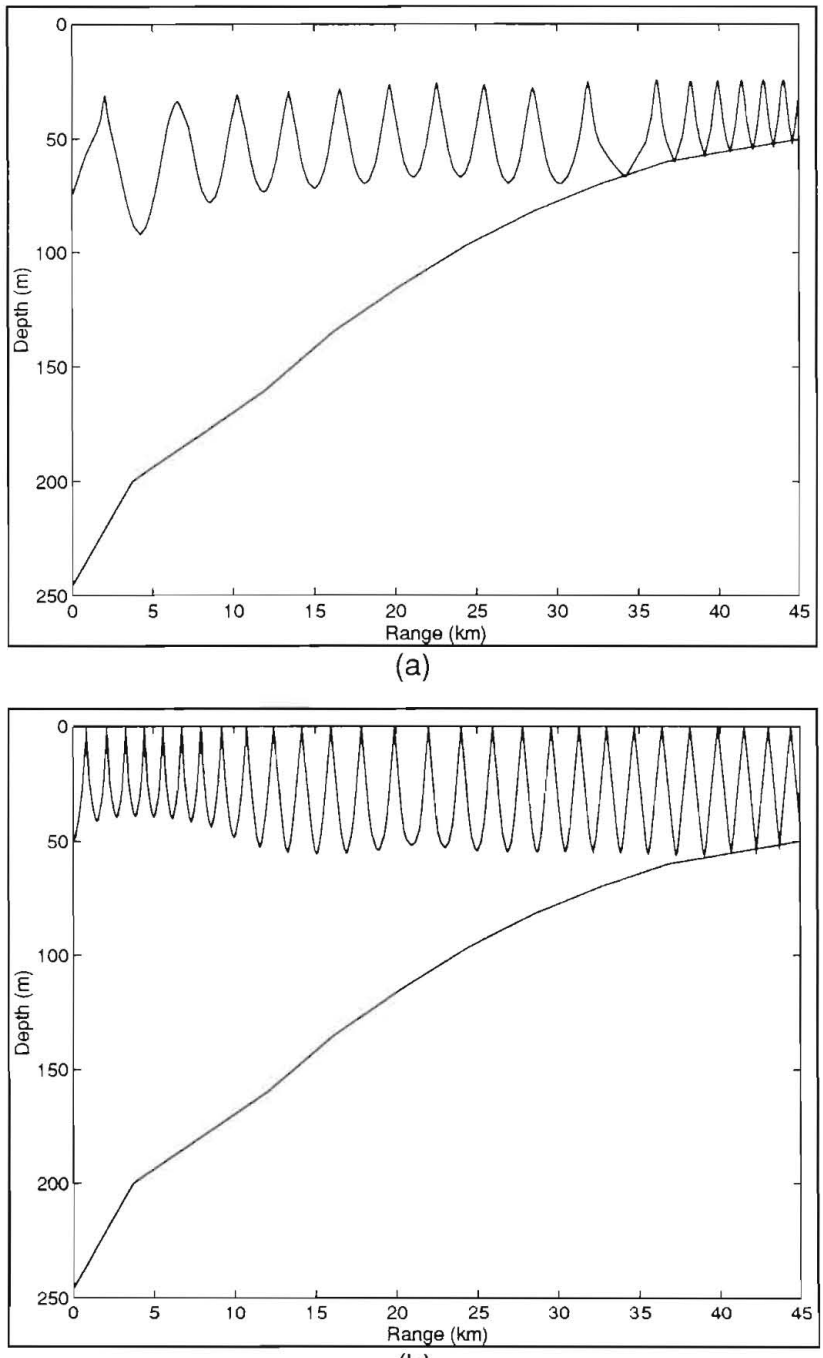

Figure 13. Ray paths for ray launched at 4° for (a) summer conditions and (b) winter conditions.

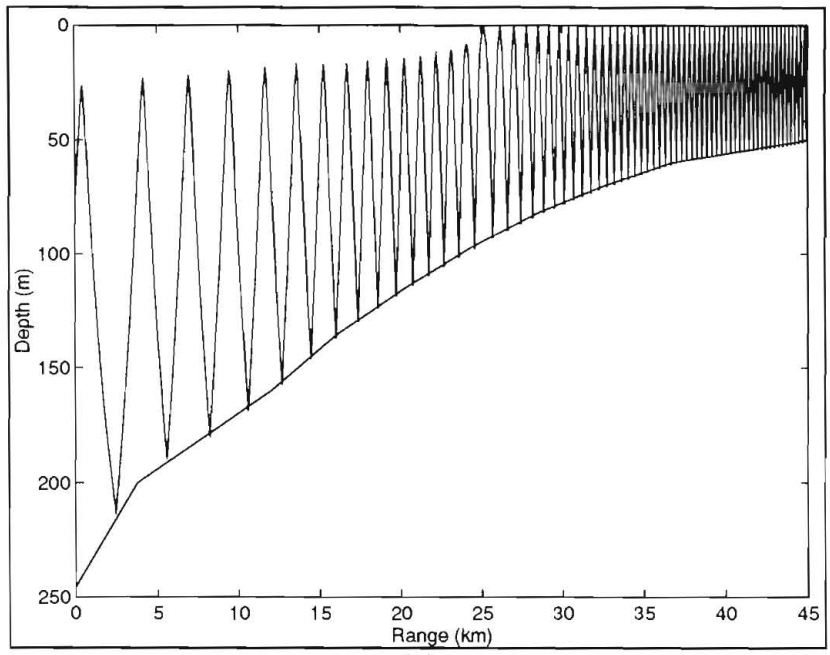

(a)

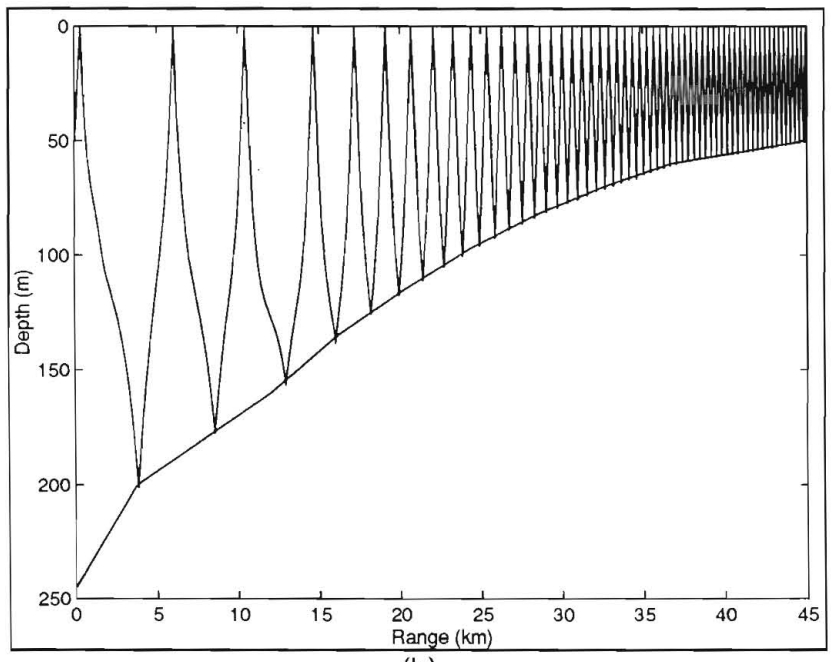

(b)

Figure 14. Ray path for ray launched at 10° for (a) summer conditions and (b) winter conditions.

range from the source to receiver array. Again using the principles of acoustic reciprocity and interchanging the source and receiver, the eigenrays obtained from the downslope HARPO runs can be used to predict the arrival structure for the actual upslope tomography experiment. The eigenray path between the source and receiver will remain the same, whereas the launch angles for the upslope runs are exactly the negative of the arrival angles from the downslope runs. Likewise the downslope launch angles can be substituted to produce the upslope arrival angles.

Figure 15 is a plot of launch angle versus arrival time for the eigenrays arriving at the eighth hydrophone from the top of the vertical receiver array located near the middle of the water column at a depth of 25.5 meters. For both summer and winter conditions a fairly symmetric pattern is noted. It is observed that the earliest arrivals for both seasons were for rays launched at low grazing angles. These rays arrive at approximately 30.4 seconds after launch in the summer and 30.7 seconds after launch during the winter. As can be seen by the number of early arrivals, energy from this first wave will completely dominate the arrival structure. As the launch angle increases, so generally does the corresponding travel time. This is expected as rays launched at steeper angles will undergo more surface and bottom interactions, thereby travelling greater overall distances. The plots indicate that the entire duration of the multipath arrival structure to the eighth hydrophone is roughly 0.7 seconds for summer conditions and 0.4 seconds for winter conditions. Analysis of all the rays traced revealed that the entire multipath arrival structure exists for 1.0 second in the summer and 0.7 seconds in the winter.

The source frequency and hardware specifications of the 400 Hz tomographic transceivers to be used in the Mid-Atlantic Bight Field Study determine the sequence period. For our specific transceivers there are 511 digits in the m-sequence code with 4 cycles per digit. The sequence period is calculated as

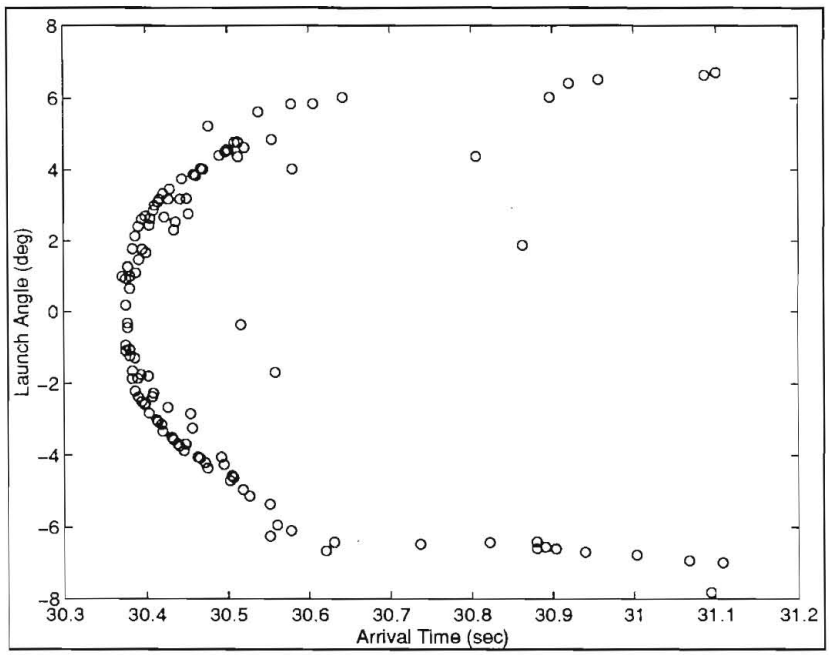

(a)

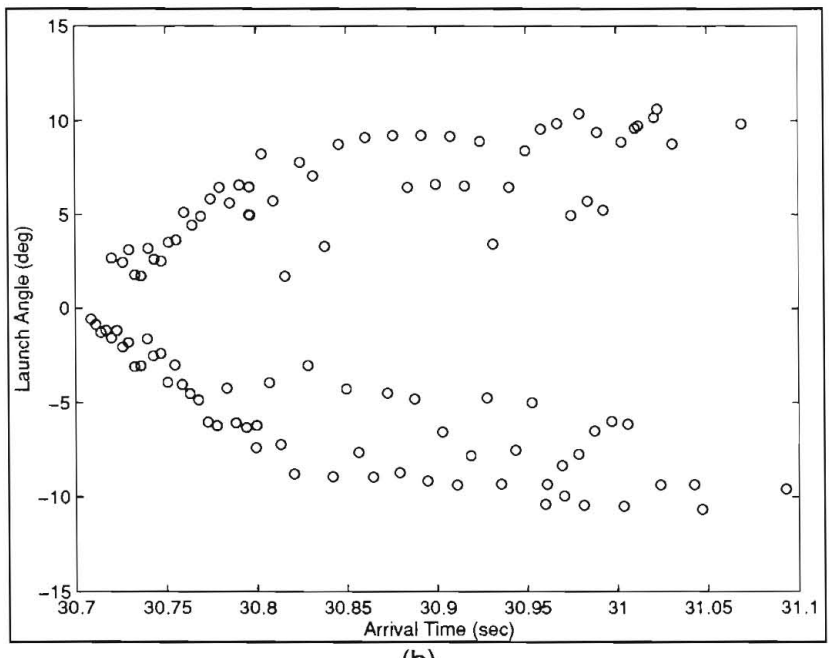

(b)

Figure 15. Launch angle versus arrival time for eigenrays to receiver hydrophone #8 for (a) summer conditions and (b) winter conditions.

$$T = \frac{1}{400Hz} * 511\ digits * 4\ \frac{cycles}{digit} = 5.11\ seconds \qquad (5.1)$$

Therefore, after 5.11 seconds the arrival pattern will repeat. With the duration of the multipath arrival structure lasting at most 1.0 second, the entire arrival structure will be observed during the sequence period.

Plots of the arrival angle versus arrival time for the summer and winter eigenrays arriving at the eighth hydrophone are provided as Figure 16. In these plots one can see that the earliest arrivals are received at low angles. In comparing Figure 16 with Figure 15, it is concluded that the greater the angle at which a ray is launched, the greater the receiving angle at the hydrophone. It is observed that the eigenrays to this particular hydrophone arrive at angles less than the critical angle of the continental shelf thereby keeping transmission loss to a minimum. Eigenrays arriving at angles greater than the critical angle would incur greater amounts of transmission loss and therefore lower signal-to-noise ratios.

The arrival structure to an individual hydrophone can be determined using the arrival time as well as amplitude and phase of the incoming signal of each eigenray. Figure 17 shows the simulated arrival structure for hydrophone #8 for both seasons. It is observed that the signal peaks with the early arrivals and drops sharply to negligent amounts. This drop occurs very rapidly after the first arrivals, 0.7 seconds for summer conditions and 0.4 seconds for winter conditions. After this drop there is very little signal in which to obtain useful information from the transmission. The analysis of similar information obtained from each hydrophone in the vertical array including launch and arrival angles, arrival time, amplitude and phase can be used to predict the complete arrival pattern. Figures 18 and 19 provide the simulated arrival structures for various hydrophones of the receiver array located throughout the water column for summer and winter conditions.

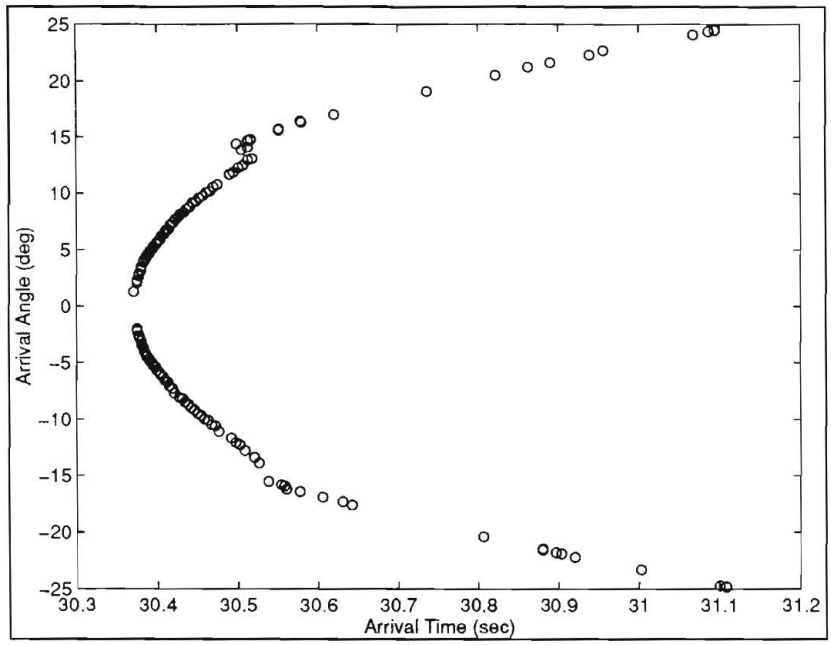

(a)

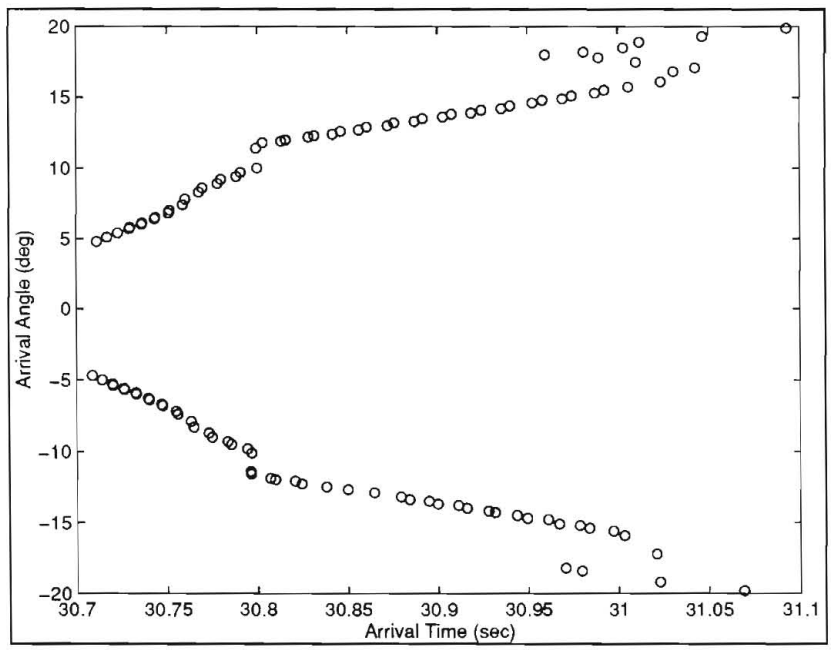

(b)

Figure 16. Arrival angle versus arrival time for eigenrays to receiver hydrophone #8 for (a) summer conditions and (b) winter conditions.

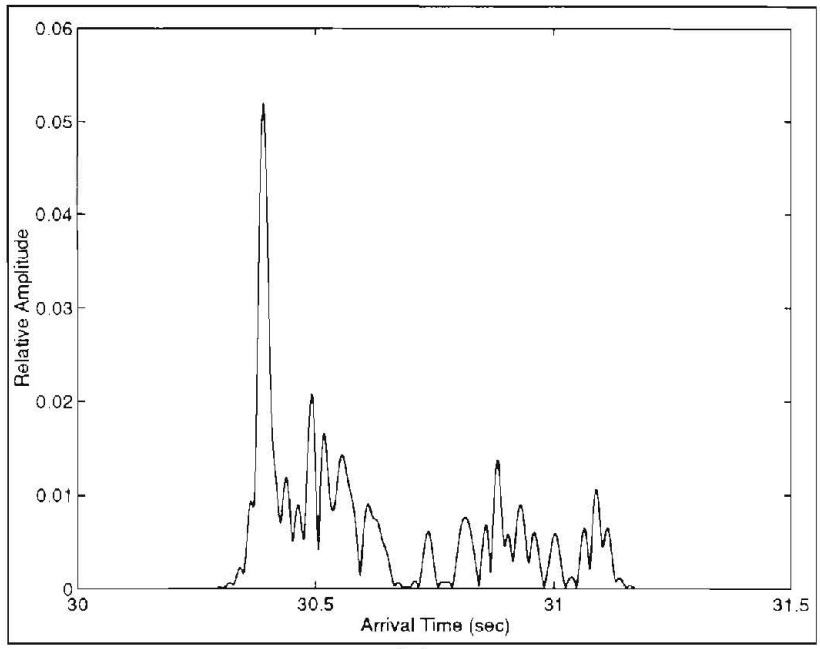

(a)

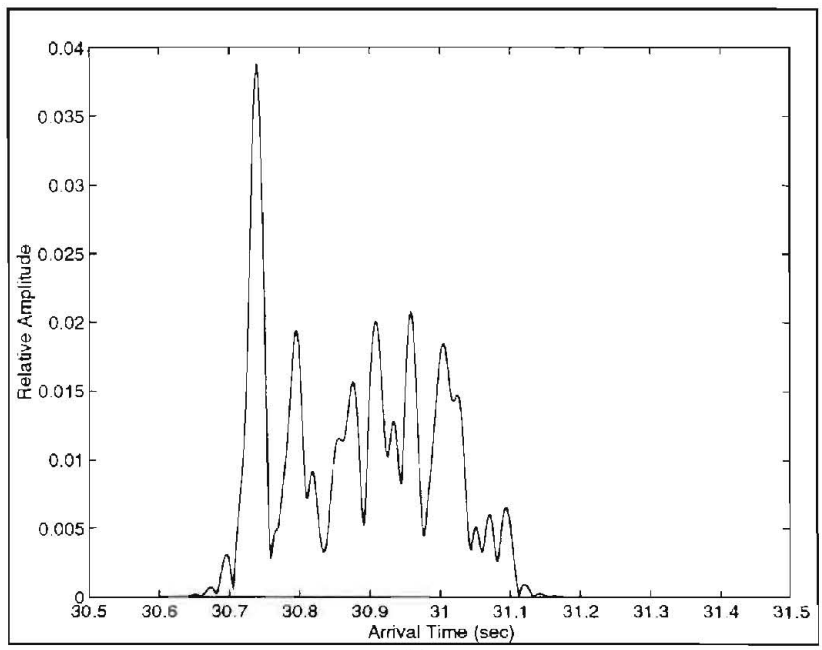

(b)

Figure 17. Simulated arrival structure at hydrophone #8 (depth 25.5 meters) for (a) summer conditions and (b) winter conditions.

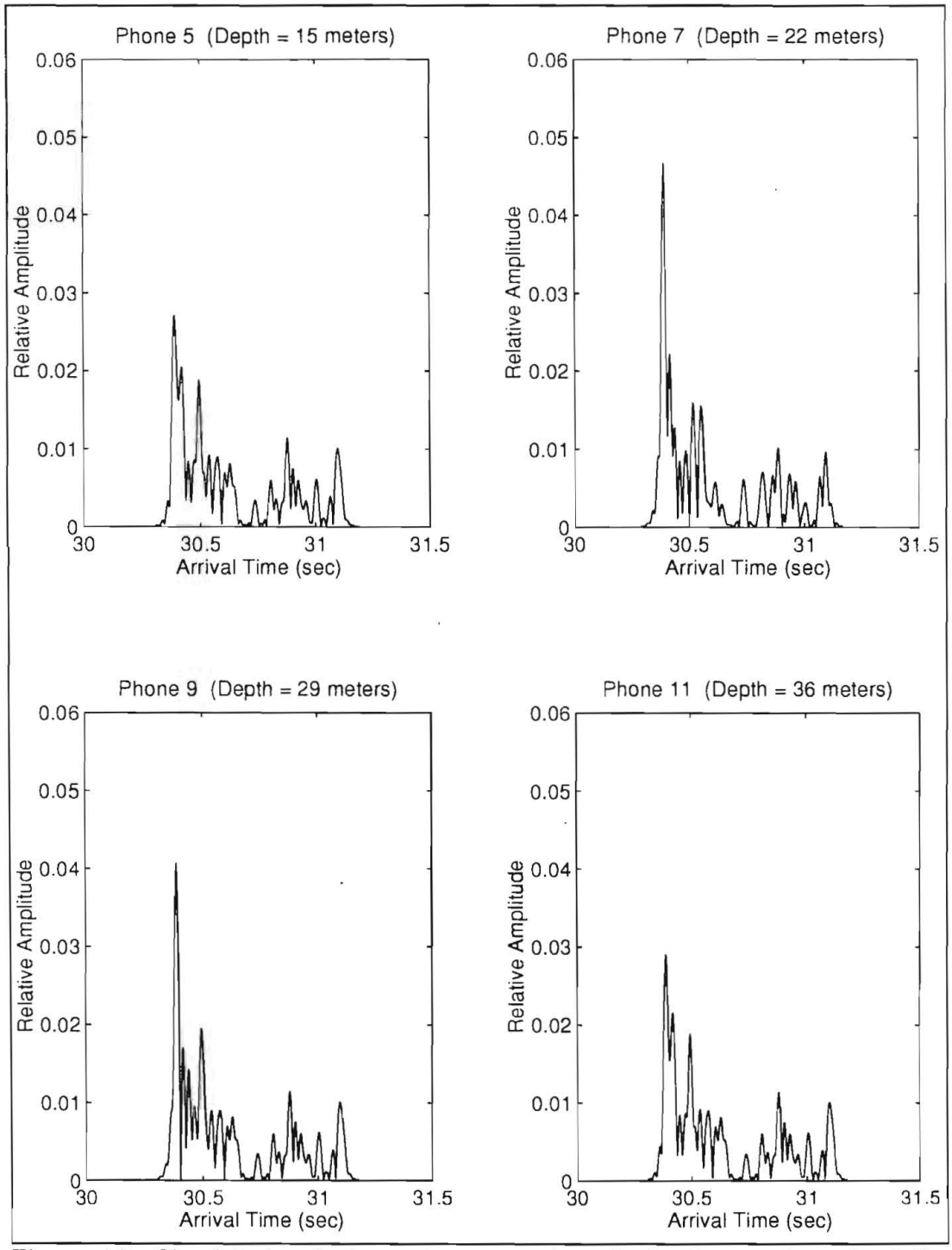

Figure 18. Simulated arrival structure at various hydrophones throughout the vertical array for summer conditions.

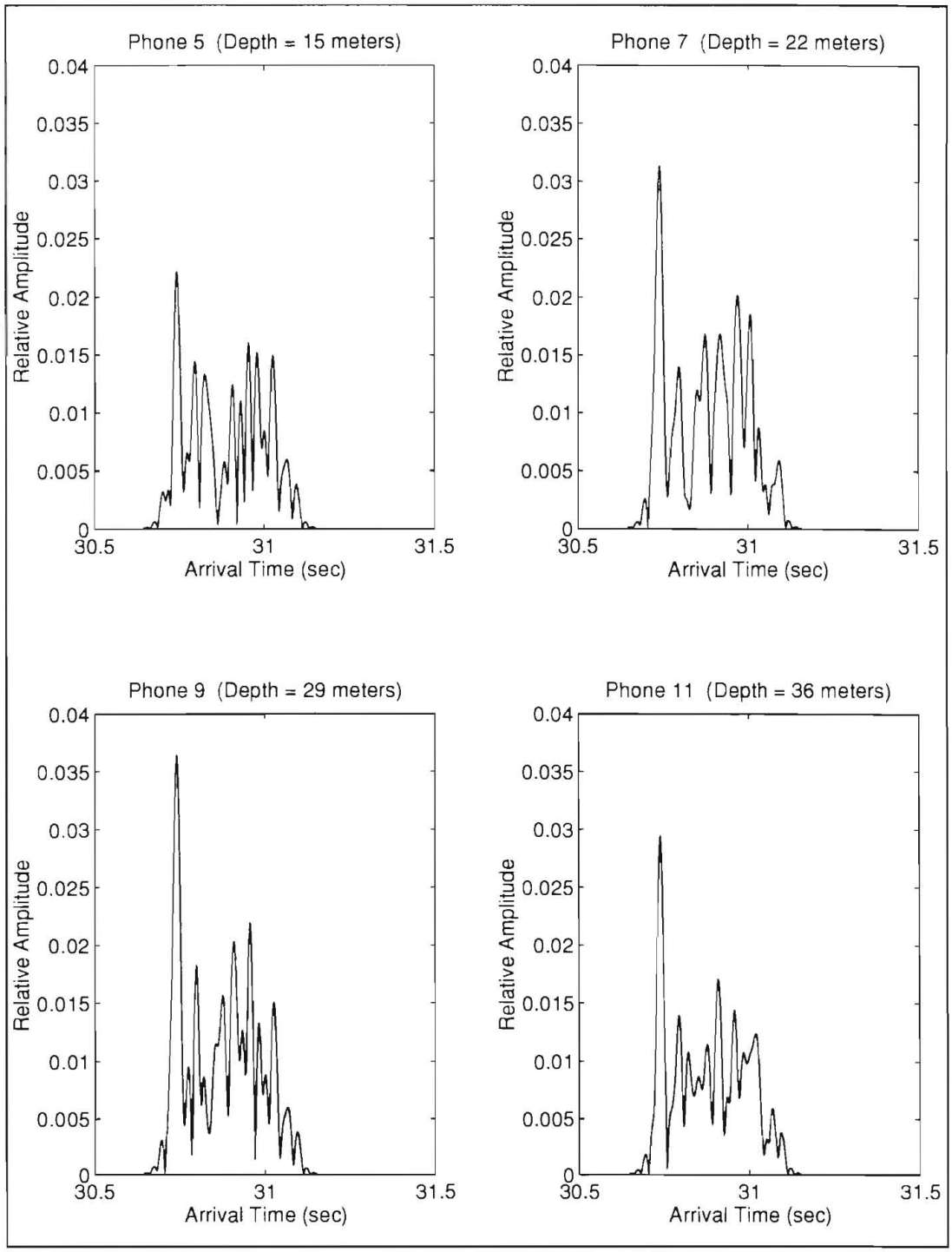

Figure 19. Simulated arrival structure at various hydrophones throughout the vertical array for winter conditions.

E. RESOLVABILITY

1. Introduction

In observing Figures 15 and 16, one can see that numerous rays arrive at the receiver array in a relatively short time frame. With so many rays arriving in such a short duration, the resolvability of individual rays becomes a question. Two separate methods were considered for resolving individual ray arrivals at the vertical receiver array. The first method used each hydrophone in the array as an independent omni-directional receiver. Resolvability in time was considered for this method. The second method used the entire receiver array as a plane wave beamformer with resolvability in time and arrival angle.

2. Individual Hydrophones

For the analysis of resolvability in time using independent hydrophones, a comparison of each eigenray arrival and its closest neighbor was conducted. If the separation in arrival time is more than the width of the transmitted pulse a ray will be resolved from all other arrivals. The bandwidth associated with the 400 Hz source signal is 100 Hz. The theoretical resolvable bin width of the transmitted pulse is 1/100 Hz or 10 milliseconds. The earliest arrivals from Figure 16 have been divided into 10 millisecond bands (Figure 20). For the earliest arrivals, especially during summer conditions, it can be seen that resolvability of individual rays will be difficult. Resolvability of the later arrivals should not pose a problem as individual rays arrivals are separated by more than 10 milliseconds in time.

3. Plane Wave Beamformer

By creating a plane wave beamformer out of the vertical array of receiver hydrophones, arrival angle in addition to arrival time can be used to resolve individual ray arrivals. To determine the angle resolution, a simple line array as outlined by Kinsler *et al.* (1982) and a plane wave beamforming method (Ziomek, 1985) for linear arrays of equally spaced point hydrophones was used.

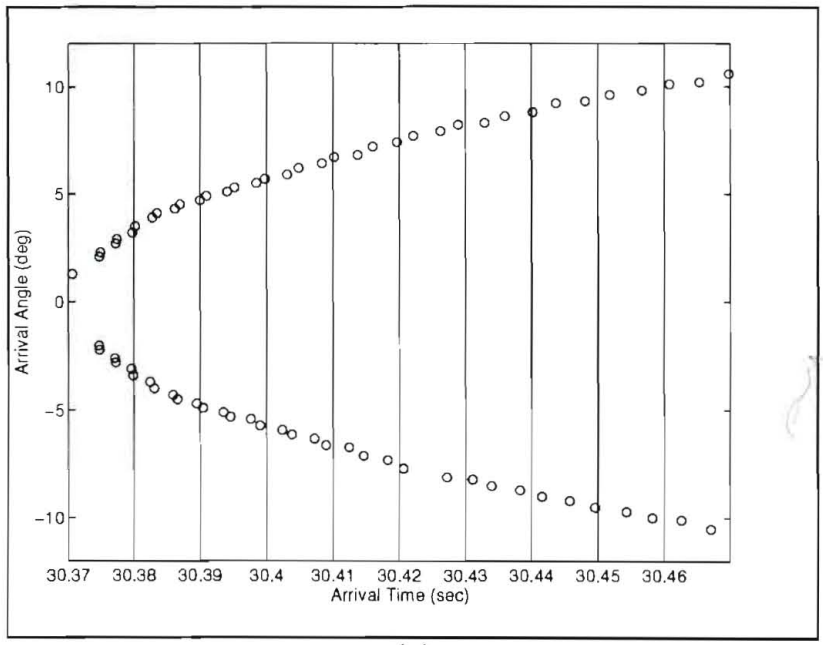

(a)

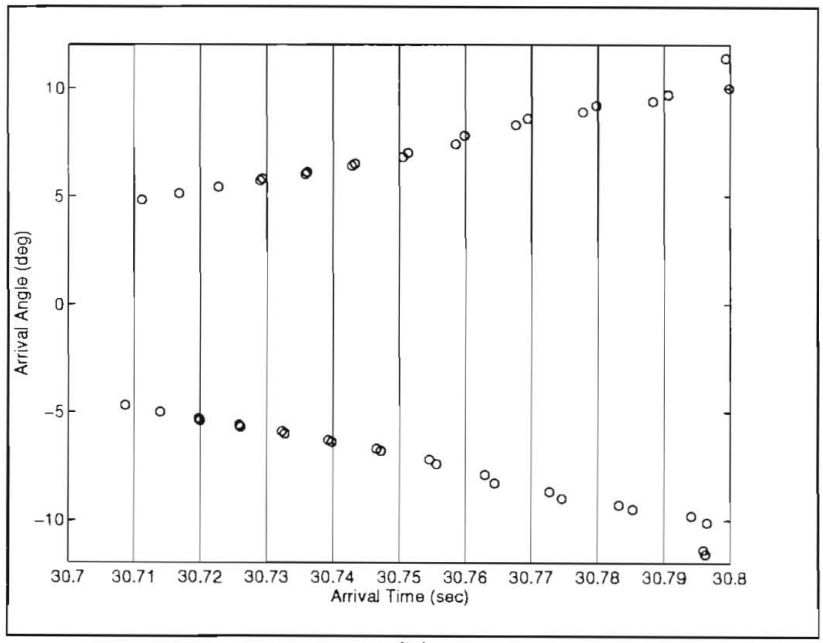

(b)

Figure 20. Arrival angle versus arrival time for early arrivals for (a) summer conditions and (b) winter conditions.

In order to obtain the greatest degree of resolvability, it is desired to have a beam pattern with a single major lobe. It is additionally desired that this single lobe be as narrow as possible. These requirements can be accomplished through the construction of the receiver array. As per Kinsler *et al.* (1982), these conditions are met by setting

$$\frac{\lambda}{d} = \frac{n}{n-1} \tag{5.2}$$

where λ is the acoustic wave length, d is the distance between hydrophones and n is the number of hydrophones. Using 15 hydrophones to receive our 400 Hz transmitted signal, a spacing requirement of 3.5 meters is established. With the given number of hydrophones at the established spacing the entire water column at the location of the receiver will be covered. This is important as ray arrivals will occur over the entire 50 meter depth.

Figure 21 provides a plot of the normalized beam pattern of the vertical array with the beam steered directly off the broadside. The beam width defined by the 3 dB down point located at 0.707 of the normalized directivity is 3.7°. Hence an angle arriving under this configuration can be resolved to ±1.85°. A plot of the normalized beam pattern for the beam steered 20° off the broadside is provided as Figure 22. The beam width for this array was found to be 4.0°. It is observed that with a steering angle a secondary main lobe, or grating lobe can appear. For this array, the grating lobe is present 68° from the steered beam. This should not cause any problems with ambiguity for any arrivals within 20° of broadside. Despite an angle resolvability of approximately ± 2.0°, Figure 18 shows that for the earliest arrivals, arrival angle for rays in the same time bin is often within the range of ± 2.0°. Therefore, resolvability of the individual rays of the early arrivals will be difficult even when utilizing both arrival time and angle. As with the individual hydrophone method, resolvability of later arrivals should pose no

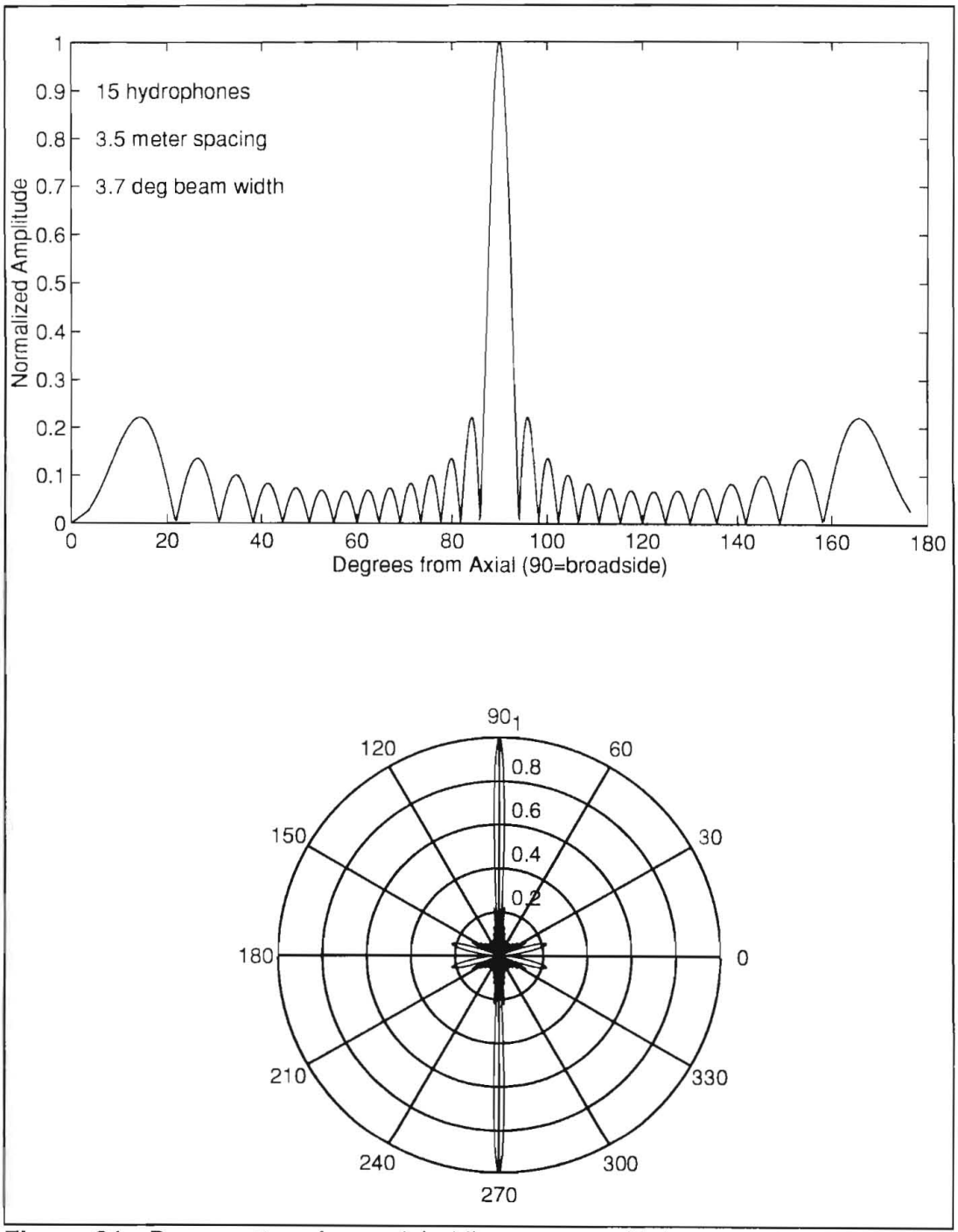

Figure 21. Beam pattern for modeled linear array with beam pattern steered off broadside.

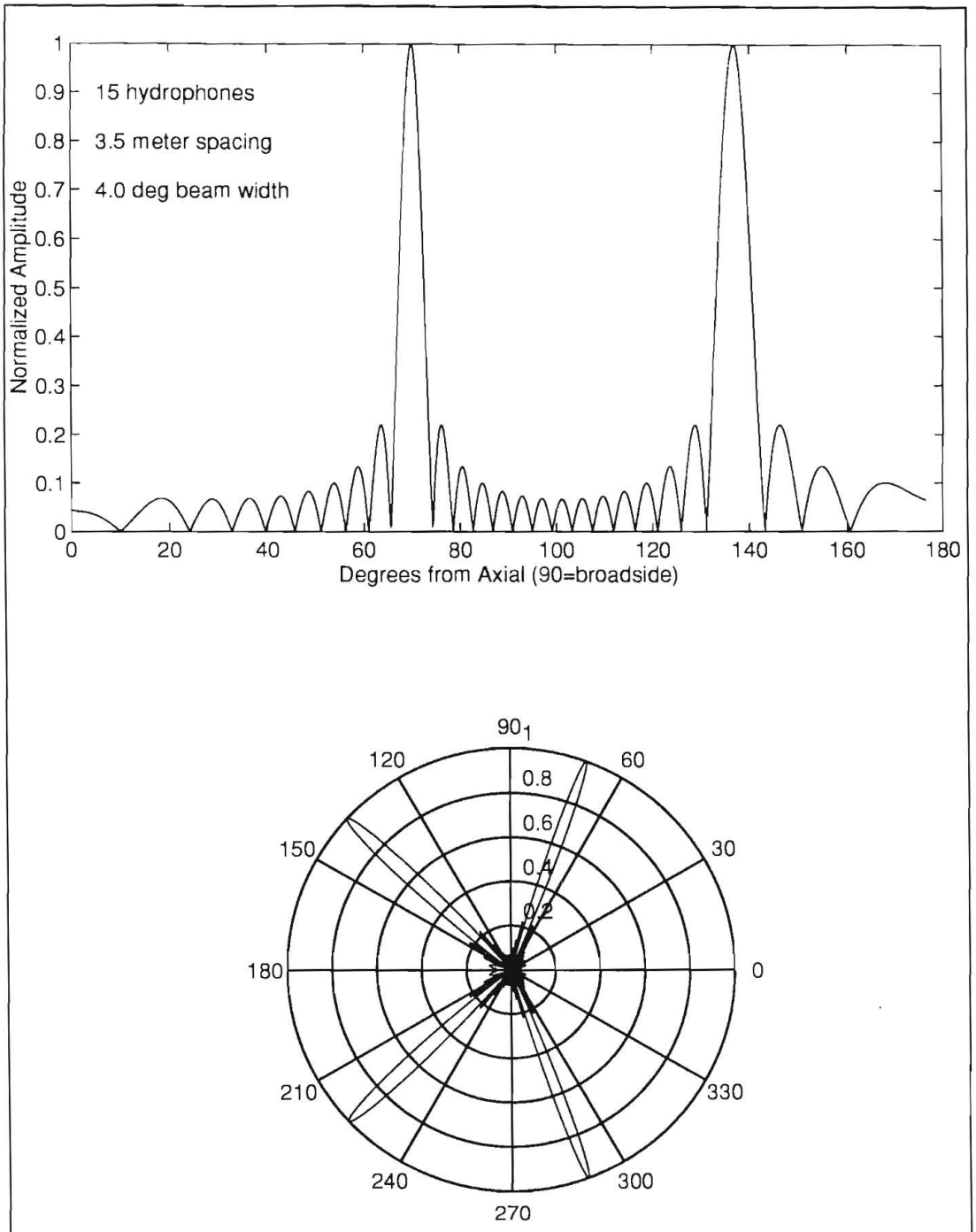

Figure 22. Beam pattern for modeled linear array with beam pattern steered 20° off broadside.

problems due to larger separations of arrival times and angles.

VI. CONCLUSIONS

The objectives of this thesis were to examine the physical oceanography of the Middle Atlantic Bight, and to evaluate, through simulations of the acoustic multipath arrival structure, the feasibility of using ocean acoustic tomography for shelf break frontal monitoring.

This summary documents major findings of the oceanographic environment of the Middle Atlantic Bight:

1. A moderate strength oceanic front is concentrated along the continental shelfbreak. Although the position of the front varies somewhat with the season and atmospheric conditions, the main axis of the front is found where the 18°C isotherm cuts the 200 meter isobath.

2. The test area is located at the separation of the continental shelf water and slope water. The shelf water in comparison with the slope water is more greatly influenced by the tides and coastal winds and has a greater spread in temperature and salinity.

3. There is a possibility of the formation of warm water rings in the test area at any time during the process studies.

4. The bottom sediment conditions are stable throughout the Middle Atlantic Bight resulting in stable bottom acoustic conditions from season to season and year to year.

5. Climate conditions are expected to be acceptable for conducting an ocean acoustic tomography test during the months of July 1996 and February 1997.

The feasibility of conducting an ocean acoustic tomography experiment is best evaluated by examining the ray path and arrival structure. This thesis examined rays which intersected a vertical plane positioned on the continental shelf located 45 kilometers from the source. Major conclusions based upon those rays include:

1. Based on the number of eigenrays and the angles from which they are launched and received, the optimal source depth is 75 meters for the summer experiment and 50 meters for the winter experiment.

2. Based on signal-to-noise ratios calculated using transmission loss, little signal is expected for rays launched at greater than ± 9.8° in the summer and ± 7.3° in the winter. Transmission loss exceeds the source level for rays launched at angles greater than ± 10.4° in the summer and ± 8.8° in the winter. As surface loss is a major source of transmission loss, a wider range of launch angles will be permitted if calmer seas than those modeled exist during the conduction of the experiments.

3. Ray path arrivals are located throughout the entire vertical water column. Based on the requirement to cover the entire water column at the receiver and to produce a beam pattern with a single narrow main lobe, hydrophone spacing was established at 3.5 meters.

4. Source frequency and hardware specifications establish a 5.11 second sequence period. As the complete multipath arrival structure is approximately 1.0 seconds during the summer and 0.7 seconds during the winter the entire multipath arrival structure will be seen during this period.

5. Arrival energy is greatest for the early arrivals due to a greater frequency of arrivals and smaller amounts of loss associated with these arrivals. Arrival structure is based on time of arrival as well as the amplitude and phase of the incoming signals. During summer conditions the most useful information obtained from the incoming signal is confined to the first 0.7 seconds, whereas this useful data lasts for 0.4 seconds during the winter.

6. Minimum time resolution is 10 milliseconds and minimum resolution in arrival angle is approximately ± 2.0°. Resolution of the individual rays in the earliest arrivals may be difficult. Modal techniques may be needed for these arrivals. Later arrivals are separated more in time and arrival angle so resolution of the individual rays should pose little problems.

LIST OF REFERENCES

Beardsley, R. C., K. H. Brink, J. Candela, M. J. Caruso, C.-S. Chiu, G. G. Gawarkiewicz, K. A. Kelly, J. F. Lynch, J. H. Miller and R. Pickart, "Sound Propagation from the Continental Slope to the Continental Shelf: an Integrated Acoustic and Oceanographic Field Study," Research Proposal submitted to the Office of Naval Research, 1994.

Chiu, C.-S., J. F. Lynch and O. M. Johannessen, "Tomographic Resolution of Mesoscale Eddies in the Marginal Ice Zone: A Preliminary Study," *Journal of Geophysical Research*, Vol. 92:C7, pp. 6886-6902, 1987.

Chiu, C.-S., A. J. Semtner, C. M. Ort, J. H. Miller and L. L. Ehret, "A Ray Variability Analysis of Sound Transmission from Heard Island to California," *The Journal of the Acoustical Society of America*, Vol. 96:4, pp. 2380-2388, 1994.

Chiu, C.-S., Department of Oceanography, Naval Postgraduate School, Monterey, CA, Personal Communication, 1995.

Clay, C. S. and H. Medwin, *Acoustical Oceanography*, John Wiley and Sons, New York, 1977.

Fairbridge, R. W., *The Encyclopedia of Atmospheric Sciences*, Reinhold Publishing Corporation, New York, 1967.

Fowles, G. R., *Analytical Mechanics, Fourth Edition*, Harcourt Brace Jovanovich College Publisher, Fort Worth, TX, 1986.

Frank, W. M. and G. M. Friedman, "Continental Shelf Sediments off New Jersey," *Journal of Sedimentary Petrology*, Vol. 43:1, pp. 224-237, 1973.

Hathaway, J. C., C. W. Poag, P. C. Valentine, R. E. Miller, D. M. Schultz, F. T. Manhiem, F. A. Kohout, M. H. Bothner, D. A. Sangrey, "U.S. Geological Survey Core Drilling on the Atlantic Shelf," *Science*, Vol. 206, pp. 515-527, 1979.

Jensen F. B., W. A. Kuperman, M. B. Porter and H. Schmidt, *Computational Ocean Acoustics*, American Institute of Physics Press, Woodbury, NY, 1994.

Jones, R. M., J. P. Riley and T. M. Georges, "HARPO: A Versatile Three-Dimensional Hamiltonian Ray Tracing Program for Acoustic Waves in an Ocean with Irregular Bottom," Wave Propagation Laboratory, National Oceanic and Atmospheric Administration, Boulder, CO, 457 pp., 1986.

Kinsler, L., A. Frey, A. Coppens and J. Sanders, *Fundamentals of Acoustics, Third Edition*, John Wiley and Sons, New York, 1982.

Knebel, H. J. and E. Speaker, "Thickness and Age of Surfical Sand Sheet, Baltimore Canyon Trough Area," *The American Association of Petroleum Geologists Bulletin*, Vol. 61:6, pp. 861-871, 1977.

Libbey-French, J., "Stratigraphic Framework and Petroleum Potential of Northeastern Baltimore Canyon Trough, Mid- Atlantic Outer Continental Shelf," *The American Association of Petroleum Geologists Bulletin*, Vol. 68:1, pp. 50-73, 1984.

Lighthill, M. J., *Waves in Fluids*, Cambridge University Press, 1978.

Miller, J. H., Department of Electrical and Computer Engineering, Naval Postgraduate School, Monterey, CA, Personal Communication, 1995.

Miller, C. W., Department of Electrical and Computer Engineering, Naval Postgraduate School, Monterey, CA, Personal Communication, 1995.

Munk, W. and C. Wunsch, "Ocean Acoustic Tomography: A Scheme for Large Scale Monitoring," *Deep Sea Research*, Vol. 26A, pp. 123-161, 1979.

Naval Oceanographic Command, "Mean Position of Ocean Fronts," NAVOCEANO Chart 5104, 1984.

Naval Oceanographic Command, International Meteorological Climate Summary Data Base, 1992.

Newhall, A. E., J. F. Lynch, C.-S. Chiu and J. R. Daugherty, "Improvements in Three-Dimensional Raytracing Codes for Underwater Acoustics," *Computational Acoustics*, Vol. 1, 1987.

O'Keefe, S., F. B. Kelso, II and C. E. Mundy, Jr., "From the Sea: Preparing the Naval Service for the 21st Century: A New Direction for the Naval Service," U.S. Navy, 1992.

Pickard, G. L. and W. J. Emery, *Descriptive Physical Oceanography*, Pergamon Press, Oxford, 1982.

Poag, C. W., "Stratigraphy and Depositional Environment of Baltimore Canyon Trough," *The American Association of Petroleum Geologists Bulletin*, Vol. 63:9, pp. 1452-1466, 1979.

Robb, J. M., J. C. Hampson, Jr. and D. C. Twichell, "Geomorphology and Sediment Stability of a Segment of the U.S. Continental Slope off New Jersey," *Science*, Vol. 211, pp. 935-937, 1981.

Schlee, J. C., "Seismic Stratigraphy of Baltimore Canyon Trough," *The American Association of Petroleum Geologists Bulletin*, Vol. 65:1, pp. 26-53, 1981.

Scripps Institute of Oceanography, *Initial Reports of the Deep Sea Drilling Project, Vol. XCV*, National Science Foundation, 1987.

Smith, K. B., M. G. Brown and F. D. Tappert, "Ray Chaos in Underwater Acoustics," *The Journal of the Acoustical Society of America*, Vol.91:4, pp.1939-1949, 1992.

Smith, K. B., Department of Physics, Naval Postgraduate School, Monterey, CA, Personal Communication, 1995.

Spindel, R. C., "Ocean Acoustic Tomography: A Review," *Current Practices and New Technology in Ocean Engineering*, Vol. 11, pp. 7-13, 1986.

Spindel, R. C., "An Underwater Acoustic Pulse Compression System," *IEEE Transactions on Acoustics, Speech and Signal Processing*, Vol. ASSP-27, No. 6, pp. 723-728, 1979.

Tchernia, P., *Descriptive Regional Oceanography*, Pergamon Press, Oxford, 1980.

Tindle, C. T. and Z. Y. Zhang, "An Equivalent Fluid Approximation for a Low Shear Speed Ocean Bottom," *The Journal of the Acoustical Society of America*, Vol. 91:6, pp.3248-3256, 1992.

Tolstoy I. and C. S. Clay, *Ocean Acoustics*, McGraw-Hill, New York, 1966.

Von Arx, W. S., *An Introduction to Physical Oceanography*, Addision-Welsey Publishing Company, Reading, MA, 1962.

Wenz, G. M., "Acoustic Ambient Noise in the Ocean: Spectra and Sources," *The Journal of the Acoustical Society of America*, Vol. 34:12, pp. 1936-1956, 1962.

Ziomek, L. J., *Underwater Acoustics: A Linear Systems Theory Approach*, Academic Press, Orlando, FL, 1985.

INITIAL DISTRIBUTION LIST

		No. Copies
1.	Defense Technical Information Center Cameron Station Alexandria, Virginia 22304-6145	2
2.	Library, Code 52 Naval Postgraduate School Monterey, California 93943-5101	2
3.	Department Chairman Code PH Department of Physics Naval Postgraduate School Monterey, California 93943-5101	1
4.	Professor James H. Miller Code EC/Mr Department of Electrical and Computer Engineering Naval Postgraduate School Monterey, California 93943-5101	5
5.	Professor Ching-Sang Chiu Code OC/Ci Department of Oceanography Naval Postgraduate School Monterey, California 93943-5101	1
6.	Professor Kevin B. Smith Code PH/Sk Department of Physics Naval Postgraduate School Monterey, California 93943-5101	1
7.	LCDR Glen E. Kaemmerer, Jr. 21 Venus Drive Belleville, Illinois 62221	2

8. Dr. James F. Lynch — 1
Department of Applied Ocean Physics and Engineering
Woods Hole Oceanographic Institution
Woods Hole, Massachusetts 02543

9. Dr. Steve Ramp — 1
Office of Naval Research
800 North Quincy Street
Arlington, Virginia 22217-5660

10. Dr. Jeff Simmen — 1
Office of Naval Research
800 North Quincy Street
Arlington, Virginia 22217-5660

11. Dr. Lou Goodman — 1
Office of Naval Research
800 North Quincy Street
Arlington, Virginia 22217-5660